Journal of Affective Disorders 354 (2024) 574–588

Contents lists available at ScienceDirect

Journal of Affective Disorders

journal homepage: www.elsevier.com/locate/jad

Research paper

Brain–gut photobiomodulation restores cognitive alterations in chronically stressed mice through the regulation of Sirt1 and neuroinflammation

Anna Sancho-Balsells [a,b,c,*], Sara Borràs-Pernas [a,b,c], Francesca Flotta [a,b,c], Wanqi Chen [a,b,c], Daniel del Toro [a,b,c], Manuel J. Rodríguez [a,b,c], Jordi Alberch [a,b,c,d], Guillaume Blivet [e], Jacques Touchon [f], Xavier Xifró [g,**], Albert Giralt [a,b,c,*]

[a] Departament de Biomedicina, Facultat de Medicina, Institut de Neurociències, Universitat de Barcelona, 08036 Barcelona, Spain
[b] Institut d'Investigacions Biomèdiques August Pi i Sunyer (IDIBAPS), 08036 Barcelona, Spain
[c] Centro de Investigación Biomédica en Red sobre Enfermedades Neurodegenerativas (CIBERNED), 28031 Madrid, Spain
[d] Production and Validation Centre of Advanced Therapies (Creatio), Faculty of Medicine and Health Science, University of Barcelona, 08036 Barcelona, Spain
[e] REGEnLIFE, 75008 Paris, France
[f] University of Montpellier, 34000 Montpellier, France
[g] New Therapeutic Targets Group, Department of Medical Science, Faculty of Medicine, Universitat de Girona, Girona, Spain

ARTICLE INFO

Keywords:
Declarative memory
Depression
hippocampus
Microglia
Microbiome

ABSTRACT

Background: Chronic stress is an important risk factor for the development of major depressive disorder (MDD). Recent studies have shown microbiome dysbiosis as one of the pathogenic mechanisms associated with MDD. Thus, it is important to find novel non-pharmacological therapeutic strategies that can modulate gut microbiota and brain activity. One such strategy is photobiomodulation (PBM), which involves the non-invasive use of light.
Objective/hypothesis: Brain-gut PBM could have a synergistic beneficial effect on the alterations induced by chronic stress.
Methods: We employed the chronic unpredictable mild stress (CUMS) protocol to induce a depressive-like state in mice. Subsequently, we administered brain-gut PBM for 6 min per day over a period of 3 weeks. Following PBM treatment, we examined behavioral, structural, molecular, and cellular alterations induced by CUMS.
Results: We observed that the CUMS protocol induces profound behavioral alterations and an increase of sirtuin1 (Sirt1) levels in the hippocampus. We then combined the stress protocol with PBM and found that tissue-combined PBM was able to rescue cognitive alterations induced by CUMS. This rescue was accompanied by a restoration of hippocampal Sirt1 levels, prevention of spine density loss in the CA1 of the hippocampus, and the modulation of the gut microbiome. PBM was also effective in reducing neuroinflammation and modulating the morphology of Iba1-positive microglia.
Limitations: The molecular mechanisms behind the beneficial effects of tissue-combined PBM are not fully understood.
Conclusions: Our results suggest that non-invasive photobiomodulation of both the brain and the gut microbiome could be beneficial in the context of stress-induced MDD.

1. Introduction

Chronic stress is considered one of modern society's most important health problems (McEwen, 2007). Chronic exposure to stressful situations has been associated with an increased risk of developing serious psychiatric disorders, including major depressive disorder (MDD) (Richter-Levin and Xu, 2018). MDD is a heterogeneous debilitating mood disorder that affects millions of people worldwide. The pathophysiology of MDD is complex, involving various altered mechanisms and systems (Tian et al., 2022). Notably, gut dysbiosis and disruptions in

Abbreviations: 4-HT, 4-Hydroxy tamoxifen; CA, Cornus Ammonis; CUMS, Chronic unpredictable mild stress; DG, Dentate gyrus; MDD, Major depression disorder; NAD+, Nicotinamide adenine dinucleotide; NOLT, Novel object location task; PBM, Photobiomodulation; Sirt1, Sirtuin 1.

* Corresponding authors at: Departament de Biomedicina, Facultat de Medicina, Institut de Neurociències, Universitat de Barcelona, Barcelona 08036, Spain.
** Correspondence to: X. Xifró, Department of Medical Science, Faculty of Medicine, Universitat de Girona, Girona, Spain.
E-mail addresses: annasanchobalsells@ub.edu (A. Sancho-Balsells), xavier.xifro@udg.edu (X. Xifró), albertgiralt@ub.edu (A. Giralt).

https://doi.org/10.1016/j.jad.2024.03.075
Received 2 February 2024; Received in revised form 6 March 2024; Accepted 10 March 2024
Available online 14 March 2024

the microbiome-gut-brain axis have emerged as key pathogenic mechanisms (Foster et al., 2017; Long-Smith et al., 2020).

Gut microbiota can be defined as the microorganisms that inhabit our gut (Cryan et al., 2018; Morais et al., 2021). Mounting evidence has revealed alterations in the gut microbiota in depressive patients (Lach et al., 2018; Mörkl et al., 2020), which has been largely confirmed in animal studies (Winter et al., 2018; Zhang et al., 2021a). However, how the microbiome can modulate brain function and behavior is still not clear. What it is known is that the microbiome influences gut-brain communication through different pathways, including the immune system. Increasing evidence shows a link between the gut microbiome and immune system function (Pearson-Leary et al., 2020; Wong et al., 2016). In this line, different rodent studies have demonstrated that microbiome dysbiosis is associated with an aberrant inflammatory response (He et al., 2024; Medina-Rodriguez et al., 2023). Therefore, it seems clear that microbial and immunological alterations could contribute to the pathophysiology of MDD.

Current MDD treatment is ineffective in approximately 30 % of patients, and it is often associated with significant side effects (Amick et al., 2015; Berlim and Turecki, 2007). Thus, the search for new therapeutic opportunities is imperative. In this regard, photobiomodulation (PBM) has emerged as a promising approach. PBM can be defined as the use of light to repair, improve, or modulate a biological function in a non-invasive way (Dompe et al., 2020). PBM in the brain has been utilized for the treatment of neurodegenerative disorders (Bathini et al., 2022; Hong, 2019) and psychiatric disorders such as MDD (Montazeri et al., 2022; Yang et al., 2021). Both depressed patients and rodent models of stress have shown beneficial effects of brain PBM (Cassano et al., 2015; Cassano et al., 2018; Maiello et al., 2019; Schiffer et al., 2009; Caldieraro and Cassano, 2019; Eshaghi et al., 2019; Gutiérrez-Menéndez et al., 2020; Mohammed, 2016; Salehpour et al., 2019a; Zhang et al., 2021b).

Although the specific molecular mechanisms underlying PBM's beneficial effects are not completely understood, several studies have shown that PBM mainly acts on the mitochondria (Dompe et al., 2020; Pan et al., 2022). Studies suggest that near-infrared light is absorbed by mitochondrial cytochrome *c* oxidase, leading to increased cellular respiration and metabolism, ATP synthesis and regulation of reactive oxygen species production, which in turn induce the activation of protective signaling pathways (Chen et al., 2022; Zhang et al., 2022). In this line, it has been proposed that Sirtuin1 (Sirt1), a nicotinamide adenine dinucleotide (NAD+)-dependent class III deacetylase, could be a key molecule involved in PBM effects (Salehpour et al., 2019b; Zhang et al., 2020; Zhu et al., 2022).

Interestingly, photobiomodulation (PBM) can exert its effect on both, the brain and the gut (Blivet et al., 2018; Hamilton et al., 2022; Wang et al., 2020). It has been proposed that PBM in the abdomen can alter gut microbiome composition (Bicknell et al., 2019), although the precise effects of PBM on the microbiome need further exploration. Consequently, the application of PBM to both the brain and the gut, referred to in this study as tissue-combined PBM or brain-gut PBM, emerges as an appealing therapeutic approach for stress-induced MDD. This dual-targeted approach has the potential to target the intricate interplay between the microbiome, immune system, and nervous system. In this line, pioneering work targeting both the brain and the gut with PBM in patients suffering from Alzheimer's disease (AD) and in AD mouse models has suggested a neuroprotective effect (Blivet et al., 2018; Blivet et al., 2022).

In the present work, we hypothesized that tissue-combined PBM targeting the brain and gut simultaneously could improve the alterations induced by chronic stress.

2. Material and methods

2.1. Animals

All mice used in the experiments were males. All mice were genotyped from a tail biopsy by PCR analysis. Mice were housed together in numerical birth order in groups of mixed genotypes (3–5 mice per cage) until starting the experiment. The animals were housed with access to food and water *ad libitum* in a colony room kept at 19–22 °C and 40–60 % humidity, under an inverted 12:12 h light/dark cycle (from 08:00 to 20:00).

For the results shown in Fig. 2, Egr1-CreER^{T2} mice were used. These mice were obtained by crossing Egr1-CreER^{T2} mice with R26RCE mice (Fig. 2C). Egr1-CreER^{T2} mice carry a bacterial artificial chromosome (BAC) including the Egr1 gene in which the coding sequence was replaced by that of the CreER^{T2} fusion protein (Longueville et al., 2021). R26RCE mice (Gt(ROSA)26Sortm1.1(CAG-EGFP)Fsh/Mmjax, Strain 004077, The Jackson Laboratory) harbor the R26R CAG-boosted EGFP (RCE) reported allele with loxP-flanked STOP cassette upstream of the enhanced green fluorescent protein (EGFP) gene.

For the other experiments, C57BL/6JOlaHsd mice from Envigo were used. All animal procedures were approved by local committees [Universitat de Barcelona, CEEA (315/18) and Generalitat de Catalunya (DAAM 10141)], following the European Communities Council Directive (86/609/EU).

2.2. Preclinical device for brain-gut photobiomodulation therapy

The PBM preclinical device (RGn530, manufactured by REGEnLIFE, Paris, France) was used to do all PBM experiments. RGn530 preclinical device is tailored to accommodate the small size of mice and designed to immobilize mice safely and securely. Thus, it considers principles of animal welfare, ensuring that mice experience minimal discomfort during the restraint period. Briefly, this apparatus is composed of 2 modules, one located at the top which exposes the head, and the other located at the bottom which exposes the abdomen (Fig. 2A). The head module is fixed because the position of the head does not vary according to the morphology of the mouse, whereas the abdomen module is adjustable to adapt to the morphology of the mouse. Each module contains a mixed emission source: lasers and LEDs. The device includes a near-infrared laser diode (850 nm), a near-infrared LED (850 nm), and a red LED (660 nm) (Fig. 2B). The photonic emissions are pulsed at a 10 Hz frequency through a ring-shaped magnet, creating a static magnetic field at 200mT. A detailed explanation of the parameters used can be found in Table 1. The two PBM treatment modules are the same for the brain and the gut and both modules emit light through an opaque funnel to narrow the light beam and deliver it precisely to the abdomen and head. To treat the animals, adult male mice were placed into a containment shuttle which is then installed into a dedicated location on the device. Therefore, the head of the mice was located under the "head module" and the abdomen was located above the "abdomen module".

Table 1
Technical specifications of the preclinical RGn530 for brain-gut PBM stimulation. Specific optical components used (and their characteristics), including wavelength, irradiance, type of emission mode, fluence, duration and number of sessions.

Component	Laser diode	IR LED	Red LED
Wavelength (nm)	**850**	**850**	**660**
Mode	Pulsed wave at 10 Hz; 50 % duty cycle		
Power density (irradiance max. – mW/cm^2)	8.86	18.50	13.23
Dose (fluence max. For 6 min. Exposure – J/cm^2)	1.59	3.33	2.38
Cumulated dose (for 15 treatments – J/cm^2)	23.85	49.95	35.7
Total number (head module)	1	1	1
Total number (abdominal module)	1	1	1

2.3. Chronic stress

To induce a depressive-like phenotype, the chronic unpredictable mild stress (CUMS) model was applied to adult male mice for 28 consecutive days. This protocol was adapted from previous work (Montalban et al., 2019; Sancho-Balsells et al., 2023). A total of seven stressors were used, which were applied randomly and once each day. The stressors used in this work include restraining, food or water deprivation, home cage inclination, forced swim, rat sawdust and light-dark cycle alteration.

2.4. Behavioral test

2.4.1. Open field and Novel object location (NOLT)

For the NOLT, an open-top arena (40 × 40 × 40 cm) with visual cues placed in the walls of the apparatus was used. Mice were first habituated to the arena (1 day, 15 min). We considered this first exposition to the open arena as an open field paradigm. We monitored the total travelled distance (in cm) as a measure of locomotor activity. On day 2, two identical objects (A1 and A2) were placed on one side of the arena and mice were allowed to explore them for 10 min. Exploration was considered when the mouse was in contact with the object and sniffed it. 24 h later (D3), one object was moved from its original location to the diagonally opposite corner and mice were allowed to explore the arena and the objects for 6 min. At the end of each trial, defecations were removed, and the apparatus was cleaned with 70 % ethanol. Animal tracking and recording were performed using the automated SMART junior 3.0 software (Panlab, Spain).

2.4.2. Y-maze

The spontaneous alternation in a Y-maze was used to determine spatial working memory. In this test, we evaluated whether mice continuously alternate (normal behavior) or, instead, they show repetitive explorative behavior. Briefly, mice were placed in the Y-shaped maze with three clear plastic arms at 120° from each other for 8 min. Around the clear Y-maze, different spatial cues were located. The total number of entries and the number of triads (% alternation) were analyzed. The % of alternation was calculated as the number of triads/number of possible triads (number of arm entries −2) *100. Arm entries were only counted if the mice placed all four limbs inside the arm.

2.4.3. Forced swim

The forced swim test was used to evaluate behavioral despair. Animals were subjected to a 6-min trial during which they were forced to swim in an acrylic glass container (35 cm height x 20 cm diameter) filled with water from which they could not escape. The time that the test animal spent in the cylinder without making any movements except those required to keep its head above water was measured and considered as “floating time”. The rest of the time was considered as time swimming/struggling.

2.4.4. Z-score

Z-score normalization was used to compare observations obtained at different behavioral tasks. As previously described (Guilloux et al., 2011) Z-scores were obtained by subtracting the average of observations in control mice from an individual raw value and then dividing this difference by the control (CNT) standard deviation. The parameters integrated into the Z-score are defined in the specific figure legend. In this work, an increase in Z-score was associated with a worse performance in the behavioral tasks, meaning mice are more affected by chronic stress.

All the tests were conducted during the light cycle and all mice were randomized throughout the day. Only one test was conducted per day.

2.5. Mass spectrometry

Hippocampal lysates were analyzed *via* mass spectrometry by the Proteomic facility at the Max Planck Institute of Biochemistry, Martinsried, Germany using label-free quantitation (LFQ) (MaxQuant run). For analysis of the data derived from mass spectrometry, the LFQ-Analyst software was used (Shah et al., 2020). Briefly, all data were filtered using a Log2 fold change of 0.5 and an adjusted *p*-value of 0.05. Benjamini Hochberg method was used for FDR correction and the MinProB imputation method was applied. EnrichR software (Kuleshov et al., 2016) was used for the analysis of differently expressed proteins.

2.6. Golgi staining

Animals were sacrificed by cervical dislocation and fresh brain hemispheres were obtained and kept in Golgi-Cox solution. After 48 h, the Golgi-Cox solution (1 % potassium dichromate, 1 % mercury chloride and 0,8 % potassium chromate) was renewed, and the brains were kept in the fresh solution for 3 weeks. Then, 200 μm slices were obtained using a vibratome (Leica VT 1000S) and processed as previously described (Ballasch et al., 2023). Secondary dendrites from CA1 pyramidal neurons were photographed using a Widefield AF6000 Monochroma Camera Leica microscope. A maximum of 3 dendrites from the same neuron were taken. *Z*-stacks from 0.2 μm were obtained in a bright field and 63× oil objective. Dendritic segments (average 30 μm) were traced with ImageJ software, and spine density was quantified. Around 50 dendrites were analyzed per condition. From each condition, 6–7 mice were quantified. Image analysis was performed blindly.

2.7. Immunofluorescence

Animals were deeply anaesthetized and subsequently intracardially perfused with 4 % (weight/vol) paraformaldehyde (PFA) in 0.1 M phosphate buffer. Brains were dissected out and kept for 48 h in 4 % PFA 0.1 M phosphate buffer in agitation. Alternatively, mice were sacrificed by cervical dislocation, and half of the brain was maintained in PFA 0.1 M for 48 h hours. After fixation, free-floating coronal sections (30 or 40 μm) were obtained using a vibratome (Leica, VT1000). Immunofluorescence was performed as previously described (Sancho-Balsells et al., 2023). Briefly, sections were washed and incubated for 30 min in 50 mM NH_4Cl. Blocking and permeabilization were performed for 1 h in PBS-T with 0.02 % azide, 3 % normal goat serum or normal donkey serum, and 0.2 % bovine serum albumin. After three washes, brain sections were incubated overnight by shaking at 4 °C with the following primary antibodies: anti-Sirt1 (1:100, Cell Signaling, #2028), MAP2 (1:500, Sigma, #M1406), Parvalbumin (1:1250, Swant, PV27), Calbindin D-28 K (1:5000, Swant, #CB38), Iba1 (1:500, Abcam, #Ab5076) GFAP (1:500, Synaptic Systems, #132006), and GFP (1:500, Abcam, #132006). All primary antibodies were diluted in the blocking solution. After three washes, sections were incubated for 2 h at room temperature with the specific fluorescent secondary AlexaFluor-488 anti-rabbit (Jackson Immuno- research, #711–545-152), AlexaFluor-488 anti-chicken (Invitrogen, #A11039), Cy3 AffiniPure anti-goat (Jackson Immunoresearch, #705–165-003), AlexaFluor-647 anti-rabbit (Invitrogen, #A31573), AlexaFluor-488 anti-goat (Invitrogen, #A32814). All secondary antibodies were diluted 1:200 in a blocking solution. Nuclei were stained for 10 min with 4′,6-diamidino-2- phenylindole (DAPI; catalogue #D9542, Sigma-Aldrich). The sections were mounted onto slides and cover slipped with Mowiol. No signal was detected in control sections incubated in the absence of the primary antibody.

2.8. Image acquisition and analysis

For GFP-positive cell counting, images were obtained in a mosaic format with a Widefield AF6000 Monochroma Camera Leica microscope with a 5× objective. To determine cell densities, the area of the *cornus*

Ammonis (CA) 1 (CA1), CA3 and dentate gyrus (DG) was delimited by comparing the original images with the Gaidi atlas. Then, the number of GFP-positive cells in a specific area was counted using the ImageJ software. The number of GFP-positive cells was relativized per area (500 μm^2). To determine the identity of the GFP-positive cells, the percentage of GFP-positive cells colocalizing with different markers (MAP2, GFAP, Parvalbumin, and Calbindin) were estimated per area as described above. For double-positive cell quantification, qualitative criteria were used. Briefly, cells presenting the expression of both markers were counted as double-positive cells. For the analysis of neuroinflammatory markers in the hippocampus, the Leica confocal SP5 was used with a 40× oil-immersion objective and a digital zoom of 2. Conditions such as pinhole size (1 AU), laser intensity, smart offset and smart gain were held constant throughout the conditions. Confocal z-stacks were taken with a z-step of 1 μm and a pixel resolution of 512 × 512. For the morphological studies carried out in microglia and astrocytes, the entire 3D stack of images was obtained using the Z drive. Images were analyzed using the freeware NIH ImageJ by Wayne Rasband (National Institutes of Health, Bethesda, MD). Microglia and astrocytes were defined automatically following the application of the *Li dark* mask and being selected by the wand tracing tool. Then the shape descriptors already present in the software were applied. For the analysis of Sirt1 levels in the hippocampus, Leica confocal SP5 was used with a x40 oil immersion objective. Conditions such as pinhole size (1 AU), laser intensity, smart offset and smart gain were held constant throughout the conditions confocal z-stacks were taken with a z-step of 5 μm and a pixel resolution of 1024 × 1024. To do the image analysis, ImageJ software was used. Briefly, the region of interest (ROI) of the CA1 or the DG was delimited with DAPI and the mean intensity of Sirt1 was calculated in the corresponding channel. For the analysis of Sirt1 intensity in astrocytes and microglia, Sirt1 intensity was measured only in GFAP in these specific cells.

2.9. Microbiome analysis

Fecal samples were collected and kept at −80° until use. Then, total genomic DNA was extracted using ZymoBIOMICS DNA Miniprep (Zymo Research, Irvine, Canada) following manufactured indications. All fecal samples were homogenized and lysate for 30 min through Vortex Genie. Qubit 4 Fluorometer (Invitrogen) was used for DNA quantification.

DNA amplicon libraries were generated targeting the 16S rRNA gene, V3-V4 regions (341F/R805) and the sequencing was performed using Illumina MiSeq PE300 following the recommendations of Illumina Inc. Sequencing was performed in Genome Québec Inc. (*Centre d'expertise et de services Génome Québec*, Montréal (Québec), Canada). The raw sequencing data were processed using QIIME (Version 22,021.2) (Bolyen et al., 2019) and pair-end reads were merged using fastq-join. Chimeric sequences were detected and deleted, meanwhile Amplicon Sequence Variant (ASV) assignment was completed using the dada2 plugin. Taxonomy was assigned at a 99 % similarity level using the q2-feature-classifier plugin with the SILVA 132 database (version 2019.10.0).

R software (Version 1.4.1717) was used for statistical analysis and plot generation. Ecological analyses were performed for alpha and beta-diversities combining *vegan, phyloseq* and *microeco* packages. For alpha diversity, the Shannon, Simpson and Chao1 index were calculated. For beta diversity, Weighted Unifrac indexes were calculated. Multivariate statistical significance analysis was carried out using PERMANOVA (Adonis2) and pairwise PERMANOVA (pairwise Adonis2) with 999 permutations ($p < 0.05$). Taxonomical distribution was represented at phylum, family, and genus level. Differential abundance analysis was performed at genus level. The ASVs counts were transformed using a centered log-ratio (CLR) approach (Mörkl et al., 2020). Differential genera were identified using ANOVA ($p < 0.05$). Correlation analysis was carried out using the genus relative abundance and Z score values of each mouse with the Pearson correlation method. All samples were processed together and by treatments with no *post-hoc* test.

2.10. Statistics

Results obtained from the behavior, Golgi staining and immunofluorescence were analyzed using GraphPad Prism software version 8.0. Data were represented as mean ± standard error of the mean (SEM). Outliers were identified with the ROUT method. Data distribution was analyzed by applying the Shapiro-Wilk normality test. Statistical analysis was performed using Student's *t*-test for comparison between two groups presenting normal distribution. For multi-component variables comparison, Kruskal-Wallis (for non-parametric data), One-way ANOVA followed by the *post-hoc* Dunn's test or Tukey's test (parametric data) or Two-way ANOVA were applied. A 95 % confidence interval was used and a *p*-value <0.05 was considered significant. The number of samples (n) and *p*-values are specified in each figure legend.

For other experiments, including proteomic analysis and microbiome sequencing, specific statistical software and methods were used. The precise details of each analysis are described in its section in the material and methods (see Mass Spectrometry and Microbiome analysis).

3. Results

3.1. Chronic stress alters mouse behavior and increases hippocampal Sirt1

We initially aimed to assess changes in mouse behavior induced by the chronic unpredictable mild stress (CUMS) protocol. Thus, mice were subjected to the CUMS protocol for 28 days (Fig. 1A), and then they were tested for several behavioral tasks. We first performed an open-field test to study locomotor activity and measure anxiety-like behavior. The results showed that CUMS mice presented increased distance travelled and spent less time in the center of the arena when compared with control (CNT) mice (Fig. 1B). These results suggest that the CUMS protocol induced hyperlocomotion and a rise in the anxiety levels. We then measured spatial working memory by evaluating the number of alternations performed in a translucid Y-maze (Fig. 1C). We observed that CUMS mice presented a decrease in the percentage of alternation when compared with CNT mice, indicating a deficit in spatial working memory. Finally, we performed a forced swim test to study behavioral despair. The results showed that CUMS mice presented a rise in the floating duration when compared with the CNT group (Fig. 1D), indicating that CUMS mice have increased despair. Altogether, these results suggest that the CUMS protocol induces profound behavioral changes in mice.

We then wanted to assess if those alterations were accompanied by proteomic changes in the hippocampus, an important brain region altered in stress-induced MDD (Tartt et al., 2022). To this end, we subjected again a new cohort of mice to the CUMS protocol and 24 h after the last stressor they were sacrificed (Fig. 1E). The hippocampus was obtained from those mice and analyzed using Mass-spectrometry technology. Using LFQ-Analyst software (Shah et al., 2020), we obtained around 80 proteins altered between both groups (Fig. 1F). Some of the differently expressed proteins included Bclaf1, Bcl2l1 and several proteins involved in the transport of substances into, out of or within the mitochondrion, such as Slc25a5, Timm9, Tmem14c, Atp5e, Mpc1 and Agt (Blake et al., 2021; Kunji et al., 2020; Mayr et al., 2010; Yien et al., 2014). The next step was to explore whether these changes in hippocampal proteins were associated with specific pathways. To do so, differently expressed proteins were subjected to a GO enrichment analysis with EnrichR to investigate underlying biological processes and signaling pathways (Kuleshov et al., 2016). We found that the Sirt1 pathway was the most significantly altered in our data analysis (*p*-value = 0.0030, odds ratio = 27.20) (Fig. 1G). Accordingly, it has been shown that Sirt1 is involved in the regulation of the expression of both, Bcl2l1 and Bclaf1 (Yu et al., 2021).

To validate the proteomic analysis and elucidate the specific

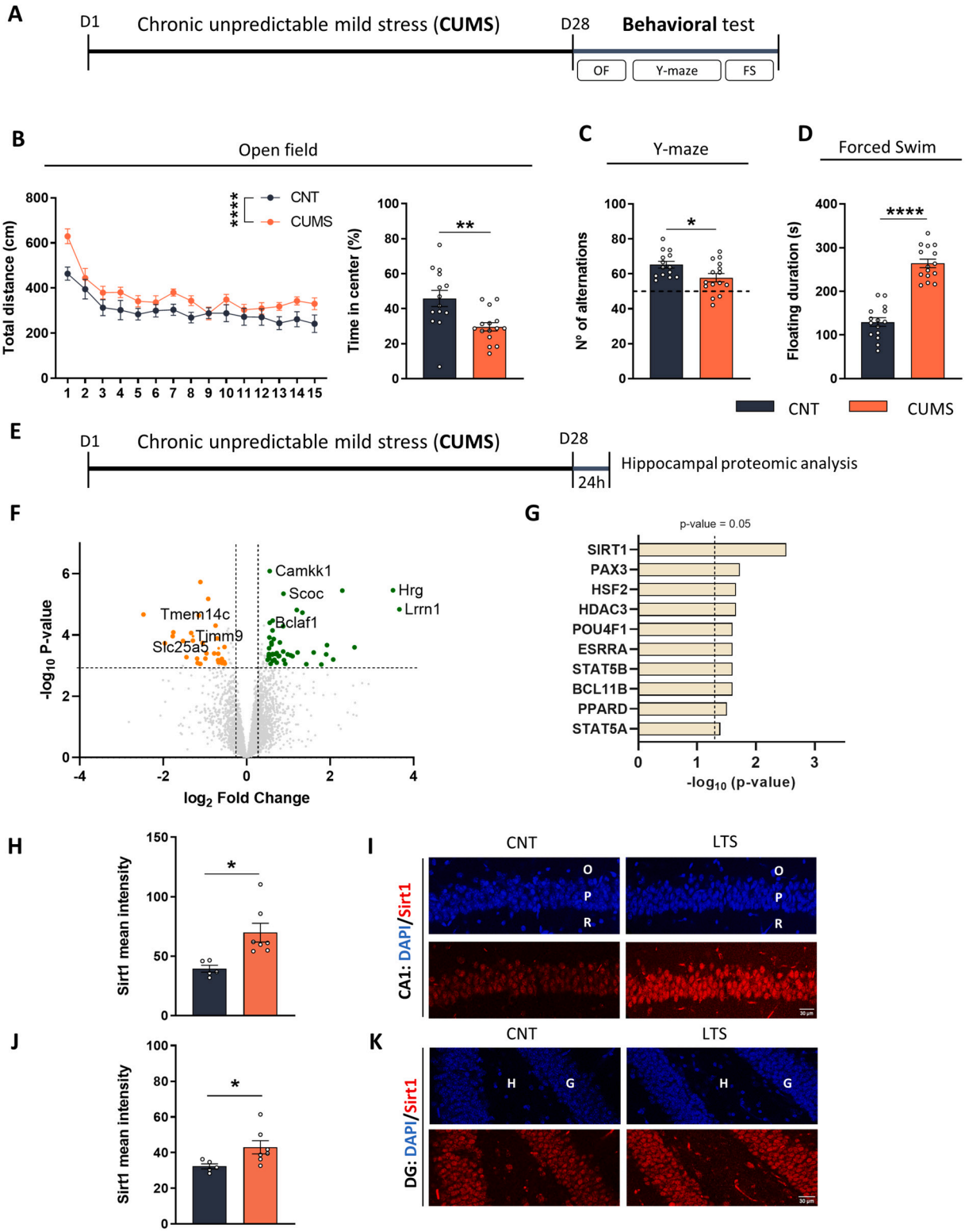

(caption on next page)

Fig. 1. Effects of the CUMS protocol on mice behavior and in the hippocampal proteome. (**A**) Schematic representation of the experimental design. 15 adult male mice were subjected to the CUMS protocol for 28 days or were kept in their homecages (CNT). At day 29, all mice were subjected to a battery of behavioral tasks. In the open field, locomotor activity and time in the center (**B**) were measured. Locomotor activity, one-way ANOVA, group effect $F(_{1,285}) = 36.67$, $P < 0.0001$. Time in the center, unpaired *t*-test: $t = 3.167$, df = 27. (**C**) Spatial working memory was studied using the translucid Y-maze. The number of alternations (%) was calculated and compared between groups, unpaired t-test: $t = 2.409$, df = 27. The dashed line indicates the chance level (50 %). In the forced swim test (**D**), floating duration during the 6 min of the test was measured. Floating duration, unpaired t-test, $t = 9.706$, df = 28. (**E**) Schematic representation of the experimental design. 7 adult male mice were subjected to the CUMS protocol and sacrificed 24 h after the last stressor. The hippocampus was obtained and analyzed using LFQ-analyst. (**F**) Volcano plot showing the differently expressed proteins between CNT and LTS mice. Data were filtered using a Log2 fold change of 0.5 and an adjusted *p*-value of 0.05. Green dots represent upregulated proteins in CNT mice, orange dots represent upregulated proteins in LTS mice and grey dots represent no significant proteins. Names of representative proteins are indicated. (**G**) Graph of the EnrichR mostly affected pathways in the enriched proteins. Sirt1 appears as the most significant pathway altered (*P*-value = 0.0030, odds ratio = 27.20). Quantification of Sirt1 levels in the CA1 (**H**) and representative images (**I**). Unpaired t-test; $p = 0.0111$, $t = 3.109$, df = 10. Quantification of Sirt1 levels in the DG (**J**) and representative images (**K**). Unpaired t-test, $p = 0.0422$, $t = 2328$, df = 10. Values are mean ± SEM. $N = 5$–7 mice/group. $^*P < 0.05$, $^{**} P < 0.005$, $^{***}P < 0.001$. D: Day; O: *Stratum Oriens*; P: *stratum pyramidale*; H: *Hilus*; G: *Stratum granulare.* (For interpretation of the references to colour in this figure legend, the reader is referred to the web version of this article.)

alterations in Sirt1 following chronic stress, total levels of Sirt1 were assessed through immunostaining in tissue sections from the mouse hippocampus. We first measured the mean intensity of Sirt1 in the CA1 and found increased levels in CUMS mice when compared with CNT mice (Fig. 1H and I). Then, we also determined Sirt1 levels in the DG and again found that CUMS samples presented higher Sirt1 immunoreactivity (Fig. 1J and K).

3.2. Photobiomodulation decreases the number of Egr1-activated neurons in the hippocampus

Having identified the Sirt1 pathway as the most altered after CUMS, and considering Sirt1 role in modulating mitochondria-related processes (Tang, 2016), we decided to manipulate its function in a non-invasive way from a translational perspective using photobiomodulation (PBM). To do so, we used a device (Fig. 2A) that allowed us to apply the PBM in specific tissues. We first aimed to identify which cells are being activated/deactivated after PBM treatment to gain insights into the underlying mechanisms. To do so, we used the Egr1-CreER^{T2}xR26RCE (Longueville et al., 2021; Sancho-Balsells et al., 2023; Brito et al., 2022) double transgenic mice (Fig. 2C) and subjected them to PBM. Briefly, mice were restrained in the apparatus and photostimulated in the head (HEAD group), in the abdomen (ABD group) or in both sites (BOTH group). The treatment consisted of 6 min of photobiomodulation from Monday to Friday for 3 weeks (Fig. 2D). On Monday of the last week, all mice received 4-hydroxy tamoxifen (4-HT) i.p. 30 min before the PBM treatment. Thus, activated cells during the PBM were labelled permanently with GFP.

In the CA1, we found a significant decrease in GFP-positive cells between CNT mice and all the other conditions (Fig. 2E). Then, in the CA3 we found the same tendency although it was only significant when comparing the HEAD group with CNT mice (Fig. 2F). We also studied the DG and found the same tendency as in the other regions, but the differences did not reach statistical significance. In summary, after PBM administration, we observed fewer Egr1-dependent activated cells in the hippocampus. Moreover, we examined if PBM treatment was inducing changes not only in the density but also in the type of activated cells. To characterize this, we immunostained the CA1 of EgrCreER^{T2}xR26RCE mice from our four conditions (CNT, HEAD, ABD and BOTH) for different markers, including MAP2, a marker for CA1 pyramidal neurons, PV, a marker of GABAergic interneurons and Calbindin, a marker of superficial neurons of the CA1. We confirmed previous data from the group as the Egr1-positive cells were all pyramidal neurons (Sancho-Balsells et al., 2023) (Supplementary Fig. 1 A and 1B). No co-localization was observed between interneurons and Egr1-positive cells (Supplementary Fig. 1 A and 1C). Then, we checked for changes in the number of deep (calbindin-negative) or superficial (calbindin-positive) neurons (Fig. 1A and D). We could not find any difference in this marker. Overall, these results suggest that although PBM causes a reduction of Egr1-positive neurons, it does not induce any cellular reorganization.

3.3. Tissue-combined photobiomodulation during chronic stress improves cognitive alterations induced by CUMS

To assess whether tissue-combined PBM could improve the alterations induced by chronic stress, the following experimental design was used. Mice underwent the CUMS protocol for 28 days or not (CNT mice). The stress protocol was combined with PBM treatment, initiated in the second week of the experiment, and applied daily (from Monday to Friday), 6 min per day (Fig. 3A). In this experimental design, five experimental groups were used (Fig. 3B). Twenty-four hours after the last stressor, fecal samples were collected for posterior microbiota studies, and mice underwent a battery of behavioral tasks (Fig. 3A).

First, we measured the total distance and the time spent in the center of the arena in the open-field test (Fig. 3C). In line with our previous results, we found that the CUMS mice presented increased distance travelled when compared with CNT mice. We also measured anxiety by calculating the time mice spent in the center of the arena. Although no significant differences were obtained, a tendency to spend less time in the center was observed in CUMS mice when compared with CNT. This tendency was abolished with the PBM treatment in the head (CUMS HEAD) and in the double-stimulated mice (CUMS BOTH), which showed levels comparable to those found in CNT mice (Fig. 3C). Then, we analyzed behavioral despair using the forced swim test. Again, all mice subjected to the CUMS protocol presented higher floating duration levels than CNT mice (Fig. 3D). No effect of PBM treatment was observed in this task either. Next, we aimed to see whether PBM could influence cognitive tasks such as the novel object location task (NOLT) and the Y-maze. In the NOLT, we first observed that CNT mice successfully discriminated between the old location (O) and the new location (N) of the object. This discrimination ability was lost in those mice that received the CUMS protocol (CUMS). Interestingly, those mice that received the double stimulation (CUMS BOTH) were also able to discriminate between objects (Fig. 3E). This result indicates that combined PBM could be beneficial for the memory alterations induced by stress. To deepen on that, we then examined spatial working memory with the Y-maze. The number of alternations between the three arms of the Y-maze was analyzed. We observed that CNT mice performed a % of alternations above those expected by chance (dashed line). Regarding the stressed mice, the only group that was not able to perform a % of alternations above the chance level was the CUMS group (Fig. 3F). This result suggests that PBM, whether applied to the head, abdomen or both locations, could be useful in mitigating spatial working memory deficits induced by chronic stress. Finally, a *Z*-score was performed to summarize the global effect of stress duration in all the behavioral tasks mentioned. As observed in Supplementary Fig. 2 A, a significant increase in Z-score was observed in all stressed groups, although the group with higher values (meaning worse behavioral performance) was the CUMS mice.

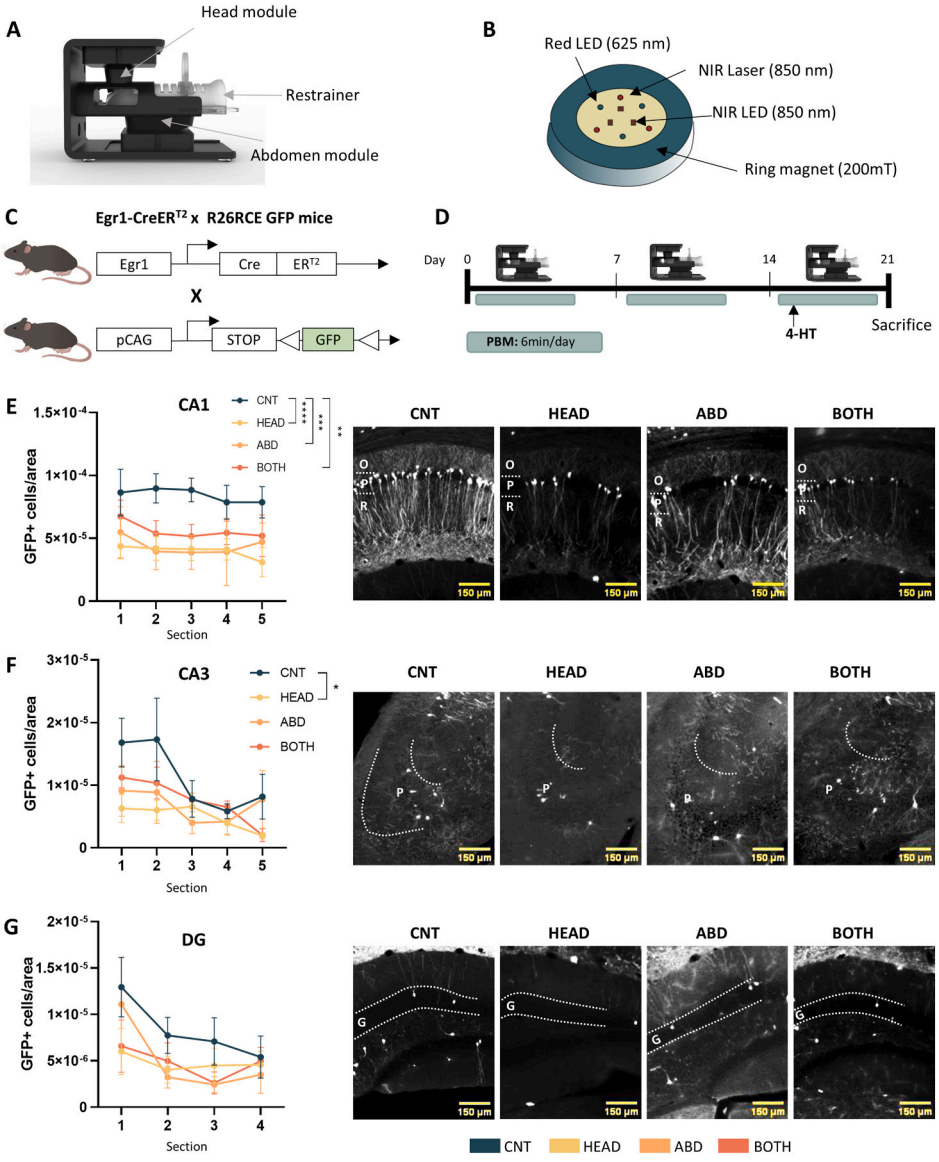

Fig. 2. Identification of active cells in different areas of the hippocampus after tissue-combined photobiomodulation. (**A**) Representative image of the photobiomodulation device, in which 2 modules are found, one in the head and one in the abdomen. Mice are placed inside the restrainer. (**B**) Schematic representation of the emission module with 1 near-infrared lasers, 1 near-infrared LEDs, 1 red LEDS and a ring magnet. (**C**) Scheme of the double heterozygous mutant Egr1-CreER^{T2} x R26RCE GFP mice. (**D**) Egr1-CreER^{T2} x R26RCE mice were placed in the photobiomodulation device and stimulated for 6 min each day. This procedure was repeated for three weeks once per day from Monday to Friday. On the first day of the last week of photobiomodulation, all mice were treated with 4-HT, 50 mg/kg, 30 min before the stimulation to induce recombination by CreER^{T2}. Representative images and quantification of Egr1-dependent activated cells (Number of GFP-positive cells/area of 500 µm^2) per region in: the CA1 (**E**), the CA3 (**F**) and the DG (**G**). In **E**, group effect, $F_{(3,64)} = 9.441$, $P < 0.001$. In **F**, group effect, $F_{(3,69)} = 3.039$, $P = 0.0347$. Tukey's test as a *post hoc* analysis was used. Values are mean ± SEM. $N = 6$–7 mice per group. P: *Stratum pyramidale*; G: *Stratum granulare*. In graphs F-G, numbers on the X-axis represent the sections analyzed (from rostral 1- to caudal 5). (For interpretation of the references to colour in this figure legend, the reader is referred to the web version of this article.)

3.4. Tissue-combined photobiomodulation regulates the gut microbiome

To determine the possible effect of stress and PBM treatment on mice microbiota, we conducted 16S ribosomal DNA sequencing. According to the principal coordinate analysis (PCoA) of beta diversity, fecal microbiota from the CUMS group was significantly different from the CNT group (Fig. 4A). No differences in beta diversity were observed between those mice receiving PBM and CNT mice. Regarding alpha diversity, no significant changes were observed between groups, as indicated by the Shannon, Simpson and Chao1 indices (Fig. 4B).

We then explored the relative phylum abundance in all groups. The taxonomy result showed that the most dominant phyla in all samples were *Bacteroidetes* and *Firmicutes* (Fig. 4C). Despite inter-individual variability, *Verrucomicrobia* was significantly increased in all the stress groups, suggesting a rise in pro-inflammatory phyla after stress (Li et al., 2017; Lin et al., 2019). To further characterize bacterial communities, we studied the relative abundance of specific genera (Fig. 4D). The five more abundant genera were analyzed. We did not observe significant changes in the abundance of specific genera, as depicted in Fig. 4D.

As only modest changes were observed, we decided to compare the levels of specific genera with the behavioral test, summarized in the *Z*-score (Supplementary Fig. 2). Consequently, the correlation between each genus abundance and the Z-score was calculated. In general, we found that the genera *Roseburia*, *Enterorhabdus, Butyricicoccus* and *Prevotellaceae NK3B31* have a significative correlation with Z score values (Supplementary Table). To further explore these correlations, the

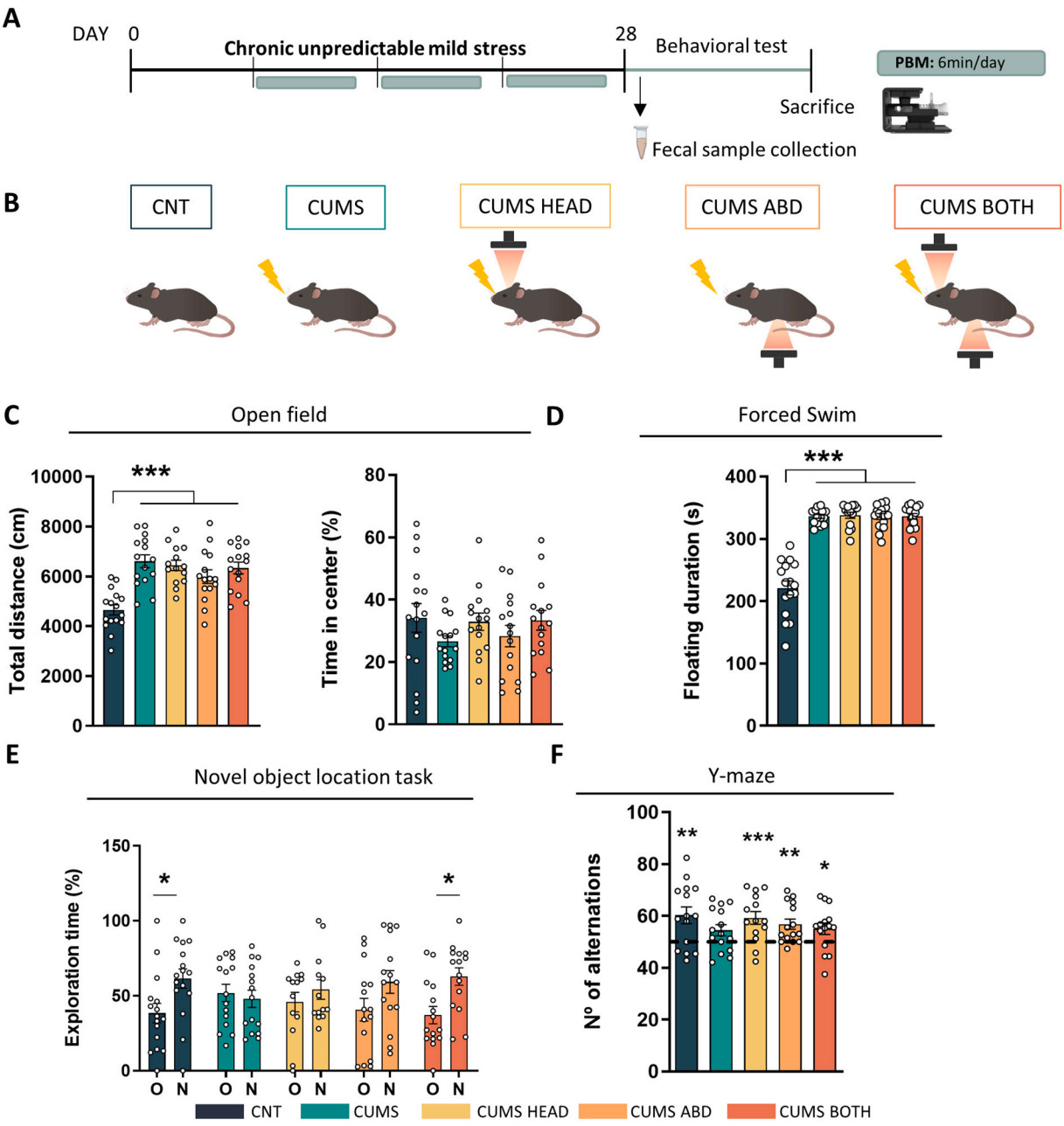

Fig. 3. PBM treatment during chronic stress improves cognitive alterations induced by CUMS. (**A**) Schematic representation of the experimental design used. Mice underwent chronic stress for 28 days (CUMS groups) or were kept in their homecages (CNT). Starting on day 8, all groups (except for CNT and CUMS) started the photobiomodulation treatment 6 min per day, from Monday to Friday. On day 29, fecal samples were collected and then mice started a battery of behavioral tests. 24 h after the last test, mice were sacrificed. (**B**) Experimental groups used for this experiment. $N = 14–16$ mice per group. The lightning symbols indicates the presence of the CUMS protocol (chronic stress). The orange light indicates PBM treatment. In the open field, total locomotor activity and time spend in the center were measured (**C**). Total distance, two-way ANOVA, group effect $F_{(4,70)} = 11.52$, $P < 0.001$. In the forced swim test (**D**), floating duration was quantified for 6 min to measured behavioral despair. $F_{(4,\ 70)} = 64.10$, $P < 0.0001$. (**E**) In the novel object location task, spatial memory was evaluated 24 h after a training trial as the percentage of total time spent exploring either the object placed at a new location (N) or the object placed at the old location (O). Two-way ANOVA, new location effect, $F_{(1,\ 138)} = 12.25$, $P = 0.0006$. (**F**) Spatial working memory was studied using the Y-maze. The number of triads (%) was calculated and compared with the chance level (50 % -dashed line). The t-test between % of alternation and 50 % was performed for each group. In **C** and **D**, Tukey as a *post hoc* analysis was used. In **E**, Bonferroni's as a *post hoc* analysis was used. All values are mean ± SEM. *P < 0.05, **P < 0.005 and ***P < 0.001.

samples were segregated by condition for a more detailed analysis (Fig. 4E). First, we observed that in CNT mice, *Roseburia* levels significantly correlated with the behavioral Z-score ($R^2 = 0.8$, *P*-value = 0.0012) and that this correlation was lost in those mice receiving the stress protocol (CUMS) ($R^2 = 0.0005$, P-value = 0.95). Interestingly, this correlation became significant in mice receiving PBM in the head (CUMS HEAD) ($R^2 = 0.47$, P-value = 0.0285) or in the head and the abdomen ($R^2 = 0.59$, P-value = 0.04) (CUMS BOTH) (Fig. 4E).

3.5. Hippocampal spine density and Sirt1 levels are recovered after PBM

As profound changes at the microbiome level associated with PBM were not identified, we turned our attention to investigating potential brain changes linked to PBM treatment. Considering the behavioral results suggesting an impact of PBM on cognitive tasks highly involving the hippocampus, we explored whether these alterations might be associated with changes in hippocampal spine density. Thus, spine

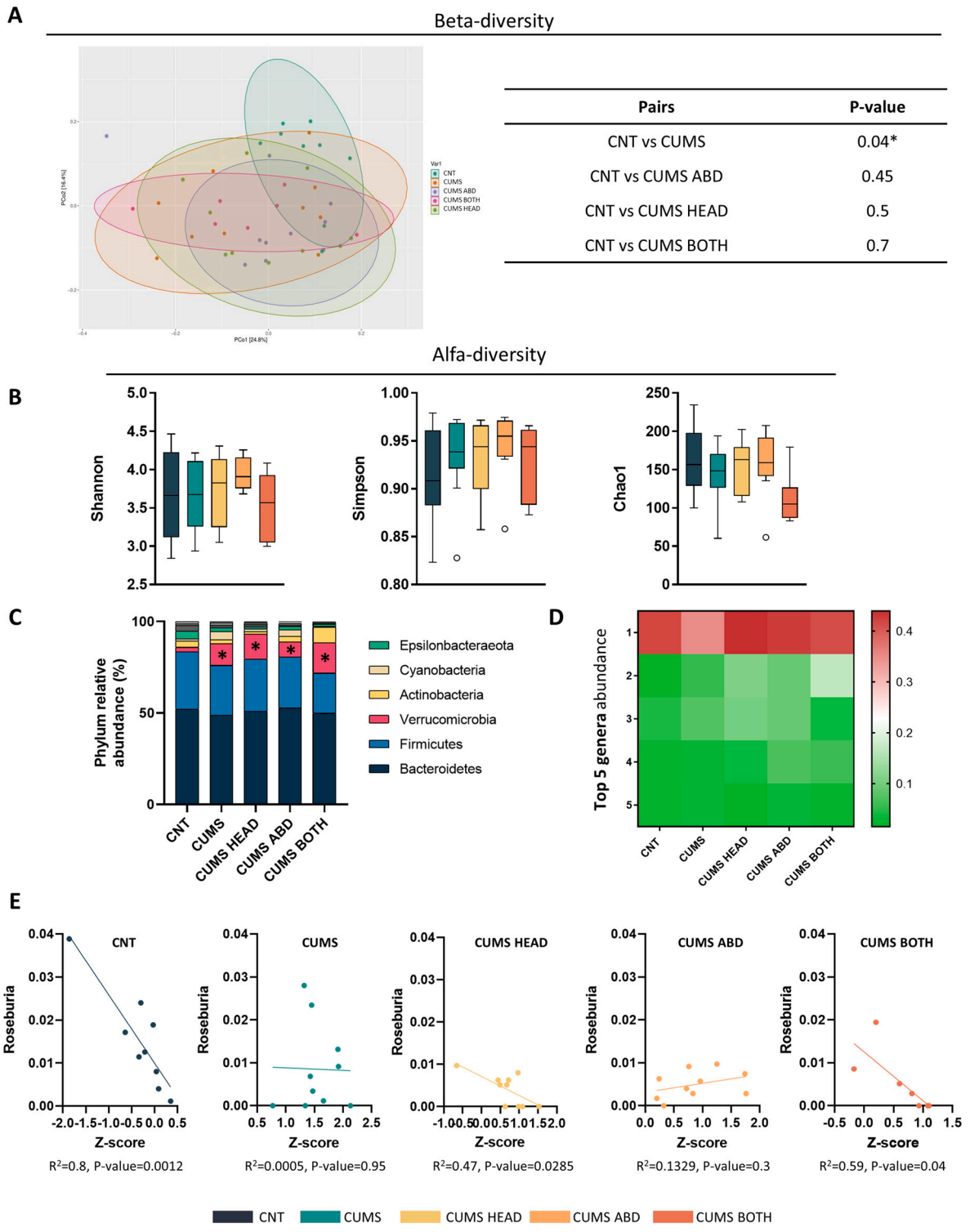

Pairs	P-value
CNT vs CUMS	0.04*
CNT vs CUMS ABD	0.45
CNT vs CUMS HEAD	0.5
CNT vs CUMS BOTH	0.7

Fig. 4. Effect of tissue-combined photobiomodulation in fecal microbiome. (**A**) Scores plot for the PCoA performed on the weighted UNIFRAC beta-diversity index grouped by treatments. Samples are colored and shaped accordingly to their type. Variance explained by each coordinate is indicated between parentheses in the corresponding axis. Table shows beta diversity statistical analysis. Significant differences (p value <0.05) between Weighted Unifrac values of sample types between treatments, calculated by pairwise PERMANOVA. (**B**) Alpha diversity of all groups did not change between groups, either with the Shannon, or Simpson or Chao1 indexes. (**C**) Relative phylum abundance in each condition. Firmicutes and Bacteroidetes were the most abundant phyla in all groups. *Verrucomicrobia* (shown in pink) was increased in all stressed conditions. (**D**) Heat map of most represented genera in all fecal samples. No statistical differences were found between groups. Numbers (1–5) represent specific genera.1: o_*Bacteroidales*, f_*Muribaculaceae*,g_ unspecified; 2: o_*Verrucomicrobiales*|f_*Akkermansiaceae*|g_*Akkermansia*; 3: o_*Lactobacillales*|f_*Lactobacillaceae*|g_*Lactobacillus*, 4: o_*Clostridiales*|f_*Lachnospiraceae*|g_*Lachnospiraceae NK4A136* group; 5: o_*Clostridiales*|f_Lachnospiraceae|g_unspecified. O: order; F: family; G: genera. (**E**) Correlation between *Roseburia* levels and the *Z*-score in CNT, CUMS, CUMS HEAD, CUMS ABD and CUMS BOTH. The coefficient of correlation and p-value associated for each correlation is depicted below the graph. (For interpretation of the references to colour in this figure legend, the reader is referred to the web version of this article.)

density was analyzed in pyramidal neurons of the CA1 of the hippocampus using the Golgi staining method. We observed a decreased spine density in CUMS mice compared to CNT mice (Fig. 5A and B). Notably, this reduction was prevented in mice subjected to PBM in the head (CUMS HEAD) and those receiving PBM in both the head and abdomen (CUMS BOTH) (Fig. 5A and B).

We then wanted to determine which molecular mechanisms could be underlying the effects of PBM. Thus, levels of Sirt1 were evaluated in the hippocampus of mice treated with PBM using immunohistochemistry. In line with our previous results (Fig. 1H), we found a significant rise in Sirt1 intensity in the CA1 of stressed mice (CUMS) when compared with the CNT group (Fig. 5C and D). This increase was prevented in those mice receiving the PBM in the abdomen (CUMS ABD) and the double stimulation (CUMS BOTH). Therefore, these results probably indicate that targeting the gut (and the microbiome resident in the gut) with PBM induces a reduction of Sirt1 levels in hippocampal neurons. We next wanted to study whether Sirt1 levels were also altered in other important hippocampal subpopulations, such as microglia and astrocytes. For this purpose, an immunofluorescence analysis was performed in the *stratum radiatum* of the hippocampus. We first noticed that Iba1-positive microglia were not expressing Sirt1 (Fig. 5E). Then, we found that GFAP-positive astrocytes were expressing Sirt1 (Fig. 5F), although no changes in Sirt1 intensity were observed in this subpopulation (Fig. 5G).

3.6. Tissue-combined photobiomodulation reduces hippocampal neuroinflammation

Despite not finding changes in Sirt1 expression in either astrocytes or

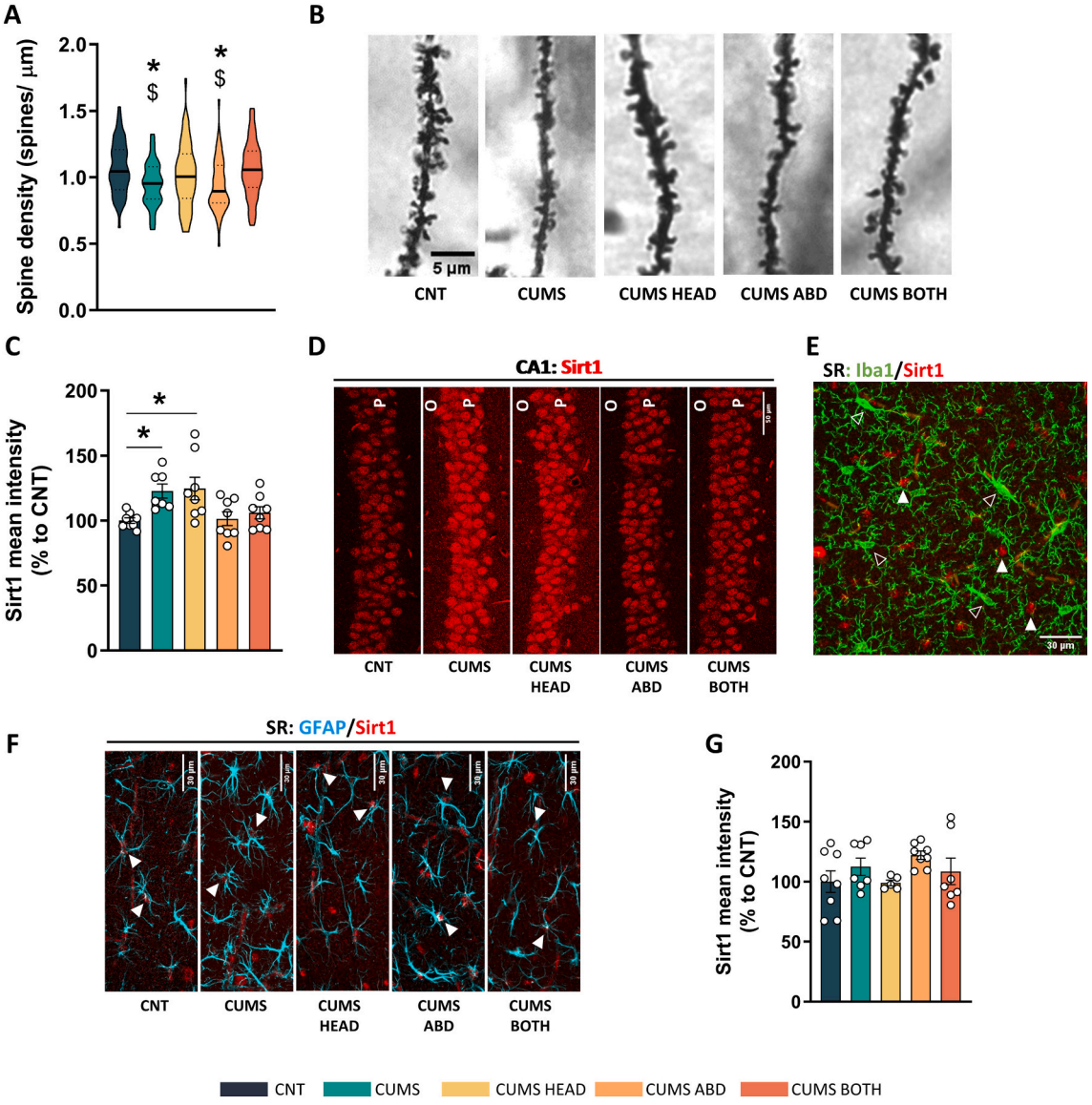

Fig. 5. Structural and molecular changes induced by PBM after CUMS. (**A**) Quantification of CA1 spine density after chronic stress and PBM treatment. One-way ANOVA, $F_{(4,255)} = 4.453$, $P = 0.0017$. Tukey's test as a *post hoc* analysis was used. $N = 50–55$ dendrites from 6 to 7 mice per group were counted. *P < 0.05 compared to CNT; $P < 0.05 compared to CUMS BOTH. (**B**) Representative images of CA1 apical dendrites from each group. (**C**) Quantification of Sirt1 mean intensity in the CA1. Two-way ANOVA, $F_{(4,34)} = 4.391$, $P = 0.0057$. Dunnett's as a *post hoc* analysis was used. *P < 0.05 compared to CNT. (**D**) Representative images of Sirt1 staining in the straum *radiatum* of the hippocampus. (**E**) Representative image of the *stratum radiatum* of the hippocampus showing Iba1-positive microglia (green) and Sirt1 expression (red). No colocalization was found between both markers. Empty arrows point to microglia cells and white arrows point to Sirt1-positive nuclei. (**F**) Representative images of the *stratum radiatum* of the hippocampus showing GFAP-astrocytes (labelled in cyan) expressing Sirt1 (in red). White arrows point to astrocytes expressing Sirt1. (**G**) Quantification of Sirt1 mean intensity in astrocytes. Values are mean ± SEM. $N = 7–8$ mice per group. O: *Stratum oriens*; P: *Stratum radiatum*. (For interpretation of the references to colour in this figure legend, the reader is referred to the web version of this article.)

microglia, we wonder if the beneficial effects observed at the behavioral level could be linked to a general effect in neuroinflammation. We evaluated the intensity and morphology of GFAP and Iba1-positive cells in the *stratum radiatum* of the CA1 of the hippocampus using immunohistochemistry. First, we observed that the intensity of GFAP was increased in the CUMS mice when compared with CNT mice. This rise was normalized with all the PBM treatments, independently of where the light was delivered (Fig. 6A and B). The same tendencies were observed when measuring GFAP intensity in each astrocyte (Fig. 6A and C). Then we further characterized if these intensity changes were accompanied by modifications in astrocyte morphology. We could not find any alteration in the GFAP cell area or GFAP circularity (Fig. 6D and E). Then, we analyzed microglia by looking at Iba1-positive cells. We first found that CUMS mice presented higher levels of total Iba1-

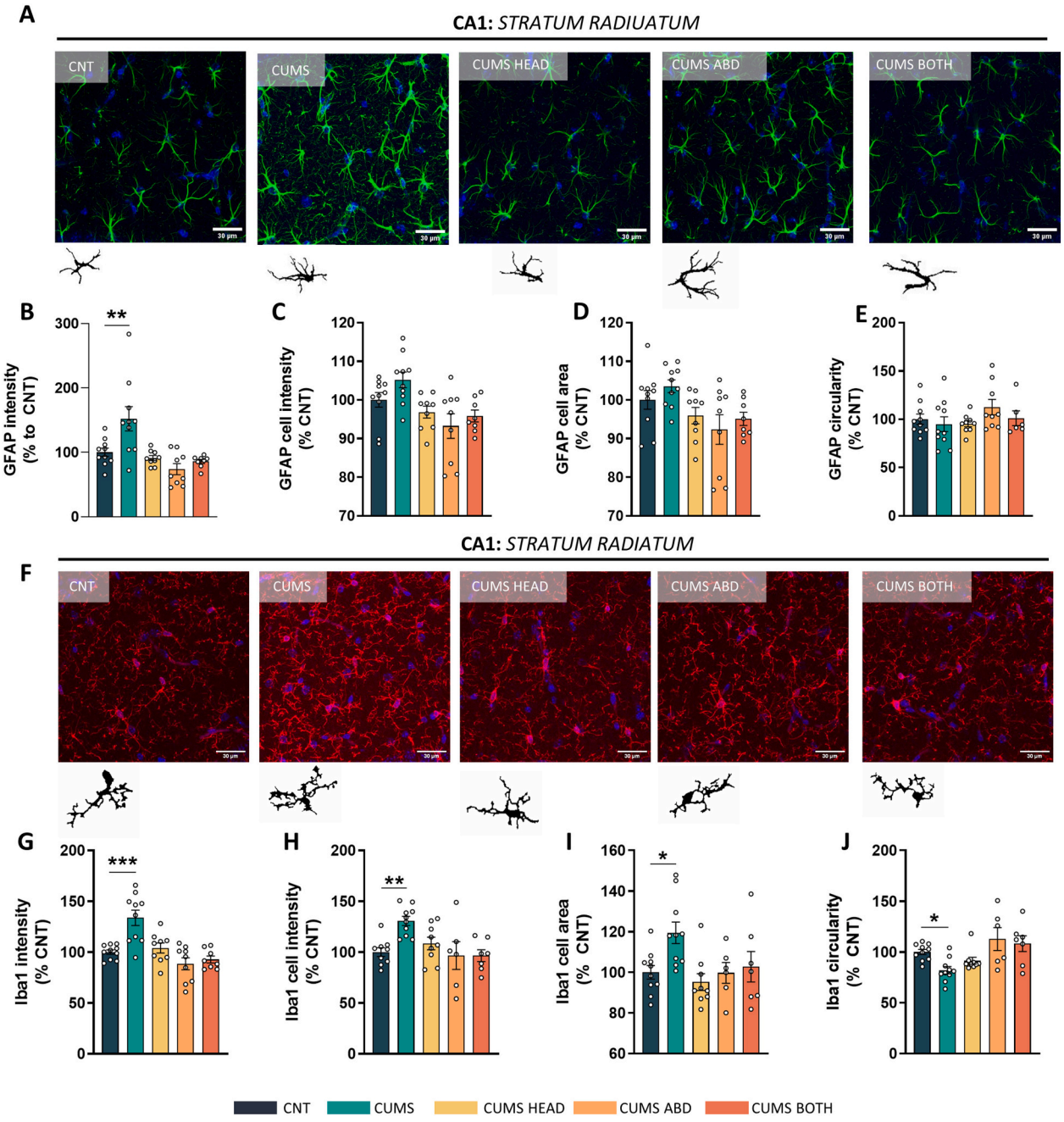

Fig. 6. Effect of tissue-combined PBM on hippocampal inflammatory markers. (**A**) Representative images of GFAP staining (green) in the *stratum radiatum* of the hippocampus in each condition. Below each picture, a representative mask of GFAP cells obtained with ImageJ is found. (**B**) Total intensity (IOD) of GFAP-positive astrocytes in the *stratum radiatum* of the hippocampus. One-way ANOVA, group factor: F (4, 41) = 8.492, P < 0.0001. (**C**) Mean intensity in each astrocyte. One-way ANOVA, group factor: $F_{(4,41)} = 4775$, $P = 0.003$. (**D**) Cell area of GFAP-positive astrocytes. (**E**) Circularity of GFAP-positive astrocytes. (**F**) Representative images of Iba1 staining (red) in the *stratum radiatum* of the hippocampus in each condition. Below each picture, a representative mask of Iba1 cells obtained with ImageJ is found. (**G**) Total intensity (IOD) of Iba1-positive microglia in the *stratum radiatum* of the hippocampus. One-way ANOVA, group factor: $F_{(4,41)} = 11.89$, P < 0.0001. (**H**) Mean intensity in each Iba1- positive microglia One-way ANOVA, group factor: $F_{(4,36)} = 5.101$, $P = 0.0023$. (**I**) Cell area of Iba1-positive microglia. One-way ANOVA, group factor: $F_{(4,37)} = 3.928$, $P = 0.0093$. (**J**) Circularity of Iba1-positive microglia. One-way ANOVA, group factor: $F_{(4, 37)} = 5204$ P = 0,0020. In **G-J**, Dunnet's as a *post hoc* analysis was used. All values are mean ± SEM. N = 6–10 mice per group. *P < 0.05, **P < 0.005 and ***P < 0.001. (For interpretation of the references to colour in this figure legend, the reader is referred to the web version of this article.)

immunoreactivity when compared with CNT mice, whereas this was prevented in those mice receiving PBM (Fig. 6F and G). This was maintained when analyzing Iba1 intensity per microglia (Fig. 6H). The morphological analysis revealed that CUMS mice presented bigger microglia, as demonstrated with a higher cell area than CNT mice. Interestingly, this was prevented with PBM treatment. Moreover, we observed that CUMS mice presented more branched microglia when compared with CNT mice (Fig. 6J) and that this was reverted with PBM.

4. Discussion

In the present work, we used tissue-combined photobiomodulation (PBM) in a mouse model of chronic unpredictable mild stress (CUMS). While PBM has been previously used for psychiatric disorders, prior research has predominantly targeted the brain. Our study aimed to stimulate both the brain and abdomen, where the microbiome is primarily located. We showed that tissue-combined PBM can be beneficial, specifically for cognitive deficits, hippocampal spine density alterations and increased neuroinflammation induced by chronic stress. Moreover, we proved that PBM can modulate the gut microbiome and correct aberrant neuronal Sirt1 expression induced by stress.

To induce an MDD-like phenotype in mice, we used the widely accepted CUMS protocol (Willner, 2017), known to induce cognitive and emotional sequelae (Montalban et al., 2019; Alqurashi et al., 2022; Avery and Silverman, 1984; Belovicova et al., 2017; Mohr et al., 2005). Considering the established connection between the hippocampus and stress-induced depression (Tartt et al., 2022; Chan et al., 2016; Frodl et al., 2002; Nifosì et al., 2010), we analyzed hippocampal proteomic changes after CUMS. We identified the Sirt1 pathway as a core molecular pathway affected in CUMS mice. We further localized such increased levels of this protein in the *stratum pyramidale* and *stratum granulosum* of the hippocampus after chronic stress. Sirt1 is a NAD+ − dependent histone deacetylase which regulates acetylation and deacetylation levels of its countless substrates. Previous literature has already described an implication of Sirt1 in stress pathologies. Whereas some papers demonstrate that Sirt1 is raised in the hippocampus (but also in other brain regions) after stress (Ferland and Schrader, 2011; Guo et al., 2021) other works suggest the opposite and describe a fall of Sirt1 expression in stress disorders (Abe-Higuchi et al., 2016; Morató et al., 2022), which illustrates the complexity of this protein function.

In the present work, we aimed to modulate Sirt1-dependent molecular changes by using a novel non-invasive photobiomodulation (PBM) approach, bringing our method closer to potential applications in human patients.

While PBM has been applied in patients, there is limited understanding of the specific brain cells regulated by this approach. To address this gap, we initially identified cells influenced by PBM by examining Egr1-dependent activated neurons. Interestingly, we found fewer activated cells after PBM in the hippocampus, suggesting that PBM modulates brain activity. In this line, previous work from the group has suggested that hippocampal Egr1 downregulation could be beneficial for stress-induced sequalae (Sancho-Balsells et al., 2023). Consequently, it is plausible to consider that the decrease in Egr1-activated neurons induced by PBM could be advantageous in stressed mice. One possible explanation for this finding is that PBM modulation of the mitochondria could lead to changes in neuronal activity. Additionally, our PBM device is surrounded and preceded by a toroid magnet, which creates a static magnetic field. Thus, we cannot rule out the possibility that the downregulation of activated cells found after PBM could be also due to this static magnetic field. In this line, some studies have shown that static magnetic fields can induce effects on the human brain and interfere with neuronal activity (Hernando et al., 2020).

Contrary to the findings of other groups, we could not find a beneficial effect of PBM in either anxiety or behavioral despair (Eshaghi et al., 2019; Zhang et al., 2021b; Meynaghizadeh-Zargar et al., 2020). This discrepancy may be attributed to variations in the optical parameters used in each PBM experiment. However, our study revealed that cognitive symptoms induced by chronic stress were either prevented or, at the very least, ameliorated through the use of a specific type of PBM that allowed simultaneous simulation of different tissues. This result was accompanied by the prevention of spine density loss in the CA1 of the hippocampus. This result aligns with previous studies wherein PBM was used to improve cognitive sequelae and increase PSD95 puncta in models of temporal lobe epilepsy and cognitive impairment (Zhang et al., 2022; Hong et al., 2023). At a molecular level, we found that the potential underlying mechanism of the PBM-dependent improvements could be the restoration of hippocampal Sirt1 levels (and probably also its function) through the stimulation of the gut. This outcome indicates somehow that gut and/or microbiome stimulation is mediating the beneficial effects of PBM regarding neuronal Sirt1 expression. Future studies should be conducted to explore how Sirt1 specifically mediates the observed beneficial effects in cognitive tasks.

To further investigate if targeting the gut and the brain with PBM could somehow modify the microbiome, the gut composition was analyzed. We first confirmed previous data supporting the idea that gut dysbiosis is present in mice that underwent chronic stress (Deng et al., 2021; Duan et al., 2021; Liu et al., 2022). Interestingly, we observed alterations in beta diversity after chronic stress, and these changes were prevented with PBM. Moreover, we presented intriguing data on the genus *Roseburia*, the levels of which correlate with mice behavioral performance in CNT, CUMS HEAD and CUMS BOTH mice. In this context, a recent study conducted on patients suffering from geriatric depression has shown that *Roseburia*, a butyrate-producing bacteria, could be involved in the remission of MDD upon specific antidepressant treatment (Lee et al., 2022). Interestingly, butyrate is a short-chain fatty acid which can inhibit several histone deacetylases, including Sirt1 (Begum et al., 2022; Schroeder et al., 2007). Thus, changes in *Roseburia* levels could, to some extent, explain the restoration of Sirt1 after PBM in both the head and abdomen.

Finally, since several studies have shown that PBM can modulate neuroinflammation in rodent models of Alzheimer's disease, autism and spinal cord injury, among others (Caldieraro and Cassano, 2019; Gutiérrez-Menéndez et al., 2020; Kim et al., 2022; Wang et al., 2021; Hamblin, 2017), we explored such pathological events in our model. We first found a punctual increase in GFAP immunoreactivity in stressed mice that was corrected after PBM stimulation. Regarding microglia, we found stronger effects and confirmed previous evidence showing increased levels of Iba1 after chronic stress (Calcia et al., 2016). Interestingly, this was significantly rescued in all PBM-treated mice. Furthermore, we observed that CUMS mice presented bigger and more branched microglia when compared with CNT mice, and these morphological changes were restored in mice treated with PBM. Supporting our findings, changes in Iba1 expression and morphology have been reported in several stress animal models (Calcia et al., 2016; Troubat et al., 2021). While it is widely acknowledged that stress exposure activates microglia, the precise mechanisms through which microglia activation leads to or contributes to the depressive phenotype remain unclear. From our results it is tempting to speculate that increased branched microglia displays higher synaptic phagocytosis activity (Hellwig et al., 2016; Mordelt and De Witte, 2023; Paolicelli et al., 2022; Wang et al., 2022) and that PBM prevented this phenotype which resulted in a restoration of the synaptic density. Moreover, since we did not detected Sirt1 in microglia, it could be hypothesized that changes in neuronal Sirt1 could somehow regulate microglia function and activation in an indirect way through the multiple described mechanisms of communication between neuronal and glial cells (Szepesi et al., 2018).

In line with our results, which indicate positive outcomes from treating both the head and abdomen separately, previous research has proposed that the beneficial effects of PBM are not limited to its impact on the brain alone; instead, they extend to the entire body (Johnstone

et al., 2015; Johnstone et al., 2014). Nevertheless, we believe that tissue-combined PBM is the most efficient approach, as it consistently demonstrates superior results across all parameters examined in this study.

5. Conclusions

In conclusion, our work suggests that tissue-combined PBM can be mostly beneficial for the cognitive deficits observed after chronic stress, probably due to the restoration of Sirt1 expression and consequent hippocampal spine density, the modulation of the microbiome and the reduction of neuroinflammation.

CRediT authorship contribution statement

Anna Sancho-Balsells: Writing – review & editing, Writing – original draft, Visualization, Validation, Methodology, Investigation, Formal analysis, Data curation, Conceptualization. **Sara Borràs-Pernas:** Methodology, Investigation, Formal analysis. **Francesca Flotta:** Investigation, Formal analysis. **Wanqi Chen:** Investigation, Formal analysis. **Daniel del Toro:** Resources, Formal analysis. **Manuel J. Rodríguez:** Data curation. **Jordi Alberch:** Writing – review & editing, Supervision. **Guillaume Blivet:** Resources, Writing – review & editing, Visualization. **Jacques Touchon:** Supervision, Resources. **Xavier Xifró:** Writing – review & editing, Supervision, Resources, Conceptualization. **Albert Giralt:** Writing – review & editing, Visualization, Validation, Supervision, Resources, Project administration, Funding acquisition, Conceptualization.

Declaration of competing interest

GB is an employee of REGEnLIFE and owns equity. JT is a consultant for REGEnLIFE. The rest of the authors declare no competing financial interests.

Data availability

All data supporting the findings of this study are available within the paper and its Supplementary Information or it is available from the authors upon reasonable request.

Acknowledgements

This work was supported by grants from Ministerio de Ciencia e Innovación/AEI/10.13039/501100011033/and "FEDER" to A.G.: PID2021-122258OB-I00 and to J.A.: PID2020-119386RB-100. Our technician Ana López, was supported by a María de Maeztu Unit of Excellence (Institute of Neurosciences, University of Barcelona, CEX2021-001159-M, Ministry of Science and Innovation). We thank María Calvo from the Advanced Microscopy Service (Centres Científics i Tecnològics Universitat de Barcelona) for her help in the acquisition, analysis, and interpretation of the confocal images. The authors also thank Dr. Aroa Relano-Gines for her support in launching the project.

Appendix A. Supplementary data

Supplementary data to this article can be found online at https://doi.org/10.1016/j.jad.2024.03.075.

References

Abe-Higuchi, N., Uchida, S., Yamagata, H., Higuchi, F., Hobara, T., Hara, K., et al., 2016. Hippocampal Sirtuin 1 signaling mediates depression-like behavior. Biol. Psychiatry 80, 815–826. https://doi.org/10.1016/j.biopsych.2016.01.009.

Alqurashi, G.K., Hindi, E.A., Zayed, M.A., Abd El-Aziz, G.S., Alturkistani, H.A., Ibrahim, R.F., et al., 2022. The impact of chronic unpredictable mild stress-induced depression on spatial, recognition and reference memory tasks in mice: behavioral and histological study. Behav. Sci. 12, 166. https://doi.org/10.3390/bs12060166.

Amick, H.R., Gartlehner, G., Gaynes, B.N., Forneris, C., Asher, G.N., Morgan, L.C., et al., 2015. Comparative benefits and harms of second generation antidepressants and cognitive behavioral therapies in initial treatment of major depressive disorder: systematic review and meta-analysis. BMJ, h6019. https://doi.org/10.1136/bmj.h6019.

Avery, D., Silverman, J., 1984. Psychomotor retardation and agitation in depression. J. Affect. Disord. 7, 67–76. https://doi.org/10.1016/0165-0327(84)90066-1.

Ballasch, I., García-García, E., Vila, C., Pérez-González, A., Sancho-Balsells, A., Fernández, J., et al., 2023. Ikzf1 as a novel regulator of microglial homeostasis in inflammation and neuro- degeneration. Brain Behav. Immun. 109, 144–161. https://doi.org/10.1016/j.bbi.2023.01.016.

Bathini, M., Raghushaker, C.R., Mahato, K.K., 2022. The molecular mechanisms of action of Photobiomodulation against neurodegenerative diseases: a systematic review. Cell. Mol. Neurobiol. 42, 955–971. https://doi.org/10.1007/s10571-020-01016-9.

Begum, N., Mandhare, A., Tryphena, K.P., Srivastava, S., Shaikh, M.F., Singh, S.B., et al., 2022. Epigenetics in depression and gut-brain axis: a molecular crosstalk. Front. Aging Neurosci. 14, 1048333 https://doi.org/10.3389/fnagi.2022.1048333.

Belovicova, K., Bogi, E., Csatlosova, K., Dubovicky, M., 2017. Animal tests for anxiety-like and depression-like behavior in rats. Interdiscip. Toxicol. 10, 40–43. https://doi.org/10.1515/intox-2017-0006.

Berlim, M.T., Turecki, G., 2007. Definition, assessment, and staging of treatment—resistant refractory major depression: a review of current concepts and methods. Can. J. Psychiatr. 52, 46–54. https://doi.org/10.1177/070674370705200108.

Bicknell, B., Liebert, A., Johnstone, D., Kiat, H., 2019. Photobiomodulation of the microbiome: implications for metabolic and inflammatory diseases. Lasers Med. Sci. 34, 317–327. https://doi.org/10.1007/s10103-018-2594-6.

Blake, J.A., Baldarelli, R., Kadin, J.A., Richardson, J.E., Smith, C.L., Bult, C.J., et al., 2021. Mouse genome database (MGD): knowledgebase for mouse–human comparative biology. Nucleic Acids Res. 49, D981–D987. https://doi.org/10.1093/nar/gkaa1083.

Blivet, G., Meunier, J., Roman, F.J., Touchon, J., 2018. Neuroprotective effect of a new photobio- modulation technique against Aβ $_{25–35}$ peptide–induced toxicity in mice: novel hypothesis for therapeutic approach of Alzheimer's disease suggested. Alzheimers Dement Transl Res Clin Interv 4, 54–63. https://doi.org/10.1016/j.trci.2017.12.003.

Blivet, G., Relano-Gines, A., Wachtel, M., Touchon, J., 2022. A randomized, double-blind, and sham-controlled trial of an innovative brain-gut Photobiomodulation therapy: safety and patient compliance. J. Alzheimers Dis. 90, 811–822. https://doi.org/10.3233/JAD-220467.

Bolyen, E., Rideout, J.R., Dillon, M.R., Bokulich, N.A., Abnet, C.C., Al-Ghalith, G.A., et al., 2019. Repro- ducible, interactive, scalable and extensible microbiome data science using QIIME 2. Nat. Biotechnol. 37, 852–857. https://doi.org/10.1038/s41587-019-0209-9.

Brito, V., Montalban, E., Sancho-Balsells, A., Pupak, A., Flotta, F., Masana, M., et al., 2022. Hippocampal *Egr1* -dependent neuronal ensembles negatively regulate motor learning. J. Neurosci. 42, 5346–5360. https://doi.org/10.1523/JNEUROSCI.2258-21.2022.

Calcia, M.A., Bonsall, D.R., Bloomfield, P.S., Selvaraj, S., Barichello, T., Howes, O.D., 2016. Stress and neuroinflammation: a systematic review of the effects of stress on microglia and the implications for mental illness. Psychopharmacology 233, 1637–1650. https://doi.org/10.1007/s00213-016-4218-9.

Caldieraro, M.A., Cassano, P., 2019. Transcranial and systemic photobiomodulation for major depressive disorder: a systematic review of efficacy, tolerability and biological mechanisms. J. Affect. Disord. 243, 262–273. https://doi.org/10.1016/j.jad.2018.09.048.

Cassano, P., Cusin, C., Mischoulon, D., Hamblin, M.R., De Taboada, L., Pisoni, A., et al., 2015. Near-infrared transcranial radiation for major depressive disorder: proof of concept study. Psychiatry J. 2015, 1–8. https://doi.org/10.1155/2015/352979.

Cassano, P., Petrie, S.R., Mischoulon, D., Cusin, C., Katnani, H., Yeung, A., et al., 2018. Transcranial Photobiomodulation for the treatment of major depressive disorder. The ELATED-2 pilot trial. Photomed. Laser Surg. 36, 634–646. https://doi.org/10.1089/pho.2018.4490.

Chan, S.W.Y., Harmer, C.J., Norbury, R., O'Sullivan, U., Goodwin, G.M., Portella, M.J., 2016. Hippocampal volume in vulnerability and resilience to depression. J. Affect. Disord. 189, 199–202. https://doi.org/10.1016/j.jad.2015.09.021.

Chen, Z., Huang, S., Liu, M., 2022. The review of the light parameters and mechanisms of Photobiomodulation on melanoma cells. Photodermatol. Photoimmunol. Photomed. 38, 3–11. https://doi.org/10.1111/phpp.12715.

Cryan, J.F., O'Riordan, K.J., Cowan, C.S.M., Sandhu, K.V., Bastiaanssen, T.F.S., Boehme, M., et al., 2018. The microbiota-gut-brain axis. Physiol. Rev. 2019 (99), 1877–2013. https://doi.org/10.1152/physrev.00018.

Deng, Y., Zhou, M., Wang, J., Yao, J., Yu, J., Liu, W., et al., 2021. Involvement of the microbiota-gut-brain axis in chronic restraint stress: disturbances of the kynurenine metabolic pathway in both the gut and brain. Gut Microbes 13, 1869501. https://doi.org/10.1080/19490976.2020.1869501.

Dompe, C., Moncrieff, L., Matys, J., Grzech-Leśniak, K., Kocherova, I., Bryja, A., et al., 2020. Photobiomodulation—underlying mechanism and clinical applications. J. Clin. Med. 9, 1724. https://doi.org/10.3390/jcm9061724.

Duan, J., Huang, Y., Tan, X., Chai, T., Wu, J., Zhang, H., et al., 2021. Characterization of gut microbiome in mice model of depression with divergent response to escitalopram treatment. Transl. Psychiatry 11, 303. https://doi.org/10.1038/s41398-021-01428-1.

Eshaghi, E., Sadigh-Eteghad, S., Mohaddes, G., Rasta, S.H., 2019. Transcranial photobiomodulation prevents anxiety and depression *via* changing serotonin and nitric oxide levels in brain of depression model mice: a study of three different doses

of 810 nm laser. Lasers Surg. Med. 51, 634–642. https://doi.org/10.1002/lsm.23082.
Ferland, C.L., Schrader, L.A., 2011. Regulation of histone acetylation in the hippocampus of chronically stressed rats: a potential role of sirtuins. Neuroscience 174, 104–114. https://doi.org/10.1016/j.neuroscience.2010.10.077.
Foster, J.A., Rinaman, L., Cryan, J.F., 2017. Stress & the gut-brain axis: regulation by the microbiome. Neurobiol Stress 7, 124–136. https://doi.org/10.1016/j.ynstr.2017.03.001.
Frodl, T., Meisenzahl, E.M., Zetzsche, T., Born, C., Groll, C., Jäger, M., et al., 2002. Hippocampal changes in patients with a first episode of major depression. Am. J. Psychiatry 159, 1112–1118. https://doi.org/10.1176/appi.ajp.159.7.1112.
Guilloux, J.-P., Seney, M., Edgar, N., Sibille, E., 2011. Integrated behavioral z-scoring increases the sensitivity and reliability of behavioral phenotyping in mice: relevance to emotionality and sex. J. Neurosci. Methods 197, 21–31. https://doi.org/10.1016/j.jneumeth.2011.01.019.
Guo, H., Deji, C., Peng, H., Zhang, J., Chen, Y., Zhang, Y., et al., 2021. The role of SIRT1 in the basolateral amygdala in depression-like behaviors in mice. Genes Brain Behav. 20, e12765 https://doi.org/10.1111/gbb.12765.
Gutiérrez-Menéndez, A., Marcos-Nistal, M., Méndez, M., Arias, J.L., 2020. Photobiomodulation as a promising new tool in the management of psychological disorders: a systematic review. Neurosci. Biobehav. Rev. 119, 242–254. https://doi.org/10.1016/j.neubiorev.2020.10.002.
Hamblin, R.M., 2017. Mechanisms and applications of the anti-inflammatory effects of photobiomodulation. AIMS Biophys 4, 337–361. https://doi.org/10.3934/biophy.2017.3.337.
Hamilton, C., Liebert, A., Pang, V., Magistretti, P., Mitrofanis, J., 2022. Lights on for autism: exploring Photobiomodulation as an effective therapeutic option. Neurol. Int. 14, 884–893. https://doi.org/10.3390/neurolint14040071.
He, H., He, H., Mo, L., You, Z., Zhang, J., 2024. Priming of microglia with dysfunctional gut microbiota impairs hippocampal neurogenesis and fosters stress vulnerability of mice. Brain Behav. Immun. 115, 280–294. https://doi.org/10.1016/j.bbi.2023.10.031.
Hellwig, S., Brioschi, S., Dieni, S., Frings, L., Masuch, A., Blank, T., et al., 2016. Altered microglia morphology and higher resilience to stress-induced depression-like behavior in CX3CR1-deficient mice. Brain Behav. Immun. 55, 126–137. https://doi.org/10.1016/j.bbi.2015.11.008.
Hernando, A., Galvez, F., García, M.A., Soto-León, V., Alonso-Bonilla, C., Aguilar, J., et al., 2020. Effects of moderate static magnetic field on neural systems is a non-invasive mechanical stimulation of the brain possible theoretically? Front. Neurosci. 14, 419. https://doi.org/10.3389/fnins.2020.00419.
Hong, N., 2019. Photobiomodulation as a treatment for neurodegenerative disorders: current and future trends. Biomed. Eng. Lett. 9, 359–366. https://doi.org/10.1007/s13534-019-00115-x.
Hong, N., Kim, H.J., Kang, K., Park, J.O., Mun, S., Kim, H.-G., et al., 2023. Photobiomodulation improves the synapses and cognitive function and ameliorates epileptic seizure by inhibiting downregulation of Nlgn3. Cell Biosci. 13, 8. https://doi.org/10.1186/s13578-022-00949-6.
Johnstone, D., Mitrofanis, J., Stone, J., 2015. Targeting the body to protect the brain: inducing neuroprotection with remotely-applied near infrared light. Neural Regen. Res. 10, 349. https://doi.org/10.4103/1673-5374.153673.
Johnstone, D.M., El Massri, N., Moro, C., Spana, S., Wang, X.S., Torres, N., et al., 2014. Indirect application of near infrared light induces neuroprotection in a mouse model of parkinsonism – an abscopal neuroprotective effect. Neuroscience 274, 93–101. https://doi.org/10.1016/j.neuroscience.2014.05.023.
Kim, U.-J., Hong, N., Ahn, J.-C., 2022. Photobiomodulation attenuated cognitive dysfunction and Neuroinflammation in a prenatal Valproic acid-induced autism Spectrum disorder mouse model. Int. J. Mol. Sci. 23, 16099 https://doi.org/10.3390/ijms232416099.
Kuleshov, M.V., Jones, M.R., Rouillard, A.D., Fernandez, N.F., Duan, Q., Wang, Z., et al., 2016. Enrichr: a comprehensive gene set enrichment analysis web server 2016 update. Nucleic Acids Res. 44, W90–W97. https://doi.org/10.1093/nar/gkw377.
Kunji, E.R.S., King, M.S., Ruprecht, J.J., Thangaratnarajah, C., 2020. The SLC25 carrier family: important transport proteins in mitochondrial physiology and pathology. Physiology 35, 302–327. https://doi.org/10.1152/physiol.00009.2020.
Lach, G., Schellekens, H., Dinan, T.G., Cryan, J.F., 2018. Anxiety, depression, and the microbiome: a role for gut peptides. Neurotherapeutics 15, 36–59. https://doi.org/10.1007/s13311-017-0585-0.
Lee, S.M., Dong, T.S., Krause-Sorio, B., Siddarth, P., Milillo, M.M., Lagishetty, V., et al., 2022. The intestinal microbiota as a predictor for antidepressant treatment outcome in geriatric depression: a prospective pilot study. Int. Psychogeriatr. 34, 33–45. https://doi.org/10.1017/S1041610221000120.
Li, H.-L., Lu, L., Wang, X.-S., Qin, L.-Y., Wang, P., Qiu, S.-P., et al., 2017. Alteration of gut microbiota and inflammatory cytokine/chemokine profiles in 5-fluorouracil induced intestinal mucositis. Front. Cell. Infect. Microbiol. 7, 455. https://doi.org/10.3389/fcimb.2017.00455.
Lin, C.-H., Chen, C.-C., Chiang, H.-L., Liou, J.-M., Chang, C.-M., Lu, T.-P., et al., 2019. Altered gut microbiota and inflammatory cytokine responses in patients with Parkinson's disease. J Neuro- inflammation 16, 129. https://doi.org/10.1186/s12974-019-1528-y.
Liu, X., Li, X., Teng, T., Jiang, Y., Xiang, Y., Fan, L., et al., 2022. Comparative analysis of gut microbiota and fecal metabolome features among multiple depressive animal models. J. Affect. Disord. 314, 103–111. https://doi.org/10.1016/j.jad.2022.06.088.
Long-Smith, C., O'Riordan, K.J., Clarke, G., Stanton, C., Dinan, T.G., Cryan, J.F., 2020. Microbiota-gut-brain Axis: new therapeutic opportunities. Annu. Rev. Pharmacol. Toxicol. 60, 477–502. https://doi.org/10.1146/annurev-pharmtox-010919-023628.
Longueville, S., Nakamura, Y., Brami-Cherrier, K., Coura, R., Hervé, D., Girault, J., 2021. Long-lasting tagging of neurons activated by seizures or cocaine administration in Egr1-CreER ^{T2} transgenic mice. Eur. J. Neurosci. 53, 1450–1472. https://doi.org/10.1111/ejn.15060.
Maiello, M., Losiewicz, O.M., Bui, E., Spera, V., Hamblin, M.R., Marques, L., et al., 2019. Transcranial photobiomodulation with near-infrared light for generalized anxiety disorder: a pilot study. Photobiomodulation Photomed Laser Surg 37, 644–650. https://doi.org/10.1089/photob.2019.4677.
Mayr, J.A., Havlickova, V., Zimmermann, F., Magler, I., Kaplanova, V., Jesina, P., et al., 2010. Mitochon- drial ATP synthase deficiency due to a mutation in the ATP5E gene for the F1 subunit. Hum. Mol. Genet. 19, 3430–3439. https://doi.org/10.1093/hmg/ddq254.
McEwen, B.S., 2007. Physiology and neurobiology of stress and adaptation: central role of the brain. Physiol. Rev. 87, 873–904. https://doi.org/10.1152/physrev.00041.2006.
Medina-Rodriguez, E.M., Cruz, A.A., De Abreu, J.C., Beurel, E., 2023. Stress, inflammation, microbiome and depression. Pharmacol. Biochem. Behav. 227–228, 173561 https://doi.org/10.1016/j.pbb.2023.173561.
Meynaghizadeh-Zargar, R., Sadigh-Eteghad, S., Mohaddes, G., Salehpour, F., Rasta, S.H., 2020. Effects of transcranial photobiomodulation and methylene blue on biochemical and behavioral profiles in mice stress model. Lasers Med. Sci. 35, 573–584. https://doi.org/10.1007/s10103-019-02851-z.
Mohammed, H.S., 2016. Transcranial low-level infrared laser irradiation ameliorates depression induced by reserpine in rats. Lasers Med. Sci. 31, 1651–1656. https://doi.org/10.1007/s10103-016-2033-5.
Mohr, P., Pecenák, J., Svestka, J., Swingler, D., Treuer, T., 2005. Treatment of acute agitation in psychotic disorders. Neuro Endocrinol. Lett. 26, 327–335.
Montalban, E., Al-Massadi, O., Sancho-Balsells, A., Brito, V., De Pins, B., Alberch, J., et al., 2019. Pyk2 in the amygdala modulates chronic stress sequelae via PSD-95-related micro-structural changes. Transl. Psychiatry 9, 3. https://doi.org/10.1038/s41398-018-0352-y.
Montazeri, K., Farhadi, M., Fekrazad, R., Chaibakhsh, S., Mahmoudian, S., 2022. Photobiomodulation therapy in mood disorders: a systematic review. Lasers Med. Sci. 37, 3343–3351. https://doi.org/10.1007/s10103-022-03641-w.
Morais, L.H., Schreiber, H.L., Mazmanian, S.K., 2021. The gut microbiota–brain axis in behaviour and brain disorders. Nat. Rev. Microbiol. 19, 241–255. https://doi.org/10.1038/s41579-020-00460-0.
Morató, L., Astori, S., Zalachoras, I., Rodrigues, J., Ghosal, S., Huang, W., et al., 2022. eNAMPT actions through nucleus accumbens NAD $^{+}$/SIRT1 link increased adiposity with sociability deficits programmed by peripuberty stress. Sci. Adv. 8, eabj9109 https://doi.org/10.1126/sciadv.abj9109.
Mordelt, A., De Witte, L.D., 2023. Microglia-mediated synaptic pruning as a key deficit in neurodevelopmental disorders: hype or hope? Curr. Opin. Neurobiol. 79, 102674 https://doi.org/10.1016/j.conb.2022.102674.
Mörkl, S., Butler, M.I., Holl, A., Cryan, J.F., Dinan, T.G., 2020. Probiotics and the microbiota-gut-brain Axis: focus on psychiatry. Curr Nutr Rep 9, 171–182. https://doi.org/10.1007/s13668-020-00313-5.
Nifosì, F., Toffanin, T., Follador, H., Zonta, F., Padovan, G., Pigato, G., et al., 2010. Reduced right posterior hippocampal volume in women with recurrent familial pure depressive disorder. Psychiatry Res. Neuroimaging 184, 23–28. https://doi.org/10.1016/j.pscychresns.2010.05.012.
Pan, L.-C., Hang, N.-L.-T., Colley, M.M.S., Chang, J., Hsiao, Y.-C., Lu, L.-S., et al., 2022. Single cell effects of photobiomodulation on mitochondrial membrane potential and reactive oxygen species production in human adipose mesenchymal stem cells. Cells 11, 972. https://doi.org/10.3390/cells11060972.
Paolicelli, R.C., Sierra, A., Stevens, B., Tremblay, M.-E., Aguzzi, A., Ajami, B., et al., 2022. Microglia states and nomenclature: a field at its crossroads. Neuron 110, 3458–3483. https://doi.org/10.1016/j.neuron.2022.10.020.
Pearson-Leary, J., Zhao, C., Bittinger, K., Eacret, D., Luz, S., Vigderman, A.S., et al., 2020. The gut microbiome regulates the increases in depressive-type behaviors and in inflammatory processes in the ventral hippocampus of stress vulnerable rats. Mol. Psychiatry 25, 1068–1079. https://doi.org/10.1038/s41380-019-0380-x.
Richter-Levin, G., Xu, L., 2018. How could stress lead to major depressive disorder? IBRO Rep 4, 38–43. https://doi.org/10.1016/j.ibror.2018.04.001.
Salehpour, F., Farajdokht, F., Cassano, P., Sadigh-Eteghad, S., Erfani, M., Hamblin, M.R., et al., 2019a. Near-infrared photobiomodulation combined with coenzyme Q10 for depression in a mouse model of restraint stress: reduction in oxidative stress, neuroinflammation, and apoptosis. Brain Res. Bull. 144, 213–222. https://doi.org/10.1016/j.brainresbull.2018.10.010.
Salehpour, F., Farajdokht, F., Mahmoudi, J., Erfani, M., Farhoudi, M., Karimi, P., et al., 2019b. Photo- biomodulation and coenzyme Q10 treatments attenuate cognitive impairment associated with model of transient global brain ischemia in artificially aged mice. Front. Cell. Neurosci. 13, 74. https://doi.org/10.3389/fncel.2019.00074.
Sancho-Balsells, A., Borràs-Pernas, S., Brito, V., Alberch, J., Girault, J.-A., Giralt, A., 2023. Cognitive and emotional symptoms induced by chronic stress are regulated by EGR1 in a subpopulation of hippocampal pyramidal neurons. Int. J. Mol. Sci. 24, 3833. https://doi.org/10.3390/ijms24043833.
Schiffer, F., Johnston, A.L., Ravichandran, C., Polcari, A., Teicher, M.H., Webb, R.H., et al., 2009. Psycho- logical benefits 2 and 4 weeks after a single treatment with near infrared light to the forehead: a pilot study of 10 patients with major depression and anxiety. Behav. Brain Funct. 5, 46. https://doi.org/10.1186/1744-9081-5-46.
Schroeder, F.A., Lin, C.L., Crusio, W.E., Akbarian, S., 2007. Antidepressant-like effects of the histone deacetylase inhibitor, sodium butyrate, in the mouse. Biol. Psychiatry 62, 55–64. https://doi.org/10.1016/j.biopsych.2006.06.036.
Shah, A.D., Goode, R.J.A., Huang, C., Powell, D.R., Schittenhelm, R.B., 2020. LFQ-analyst: an easy-to-use interactive web platform to analyze and visualize label-free

proteomics data preprocessed with MaxQuant. J. Proteome Res. 19, 204–211. https://doi.org/10.1021/acs.jproteome.9b00496.
Szepesi, Z., Manouchehrian, O., Bachiller, S., Deierborg, T., 2018. Bidirectional microglia–neuron communication in health and disease. Front. Cell. Neurosci. 12, 323. https://doi.org/10.3389/fncel.2018.00323.
Tang, B.L., 2016. Sirt1 and the mitochondria. Mol. Cell 39, 87–95. https://doi.org/10.14348/molcells.2016.2318.
Tartt, A.N., Mariani, M.B., Hen, R., Mann, J.J., Boldrini, M., 2022. Dysregulation of adult hippocampal neuroplasticity in major depression: pathogenesis and therapeutic implications. Mol. Psychiatry 27, 2689–2699. https://doi.org/10.1038/s41380-022-01520-y.
Tian, H., Hu, Z., Xu, J., Wang, C., 2022. The molecular pathophysiology of depression and the new therapeutics. MedComm 3, e156. https://doi.org/10.1002/mco2.156.
Troubat, R., Barone, P., Leman, S., Desmidt, T., Cressant, A., Atanasova, B., et al., 2021. Neuroinflammation and depression: a review. Eur. J. Neurosci. 53, 151–171. https://doi.org/10.1111/ejn.14720.
Wang, H., He, Y., Sun, Z., Ren, S., Liu, M., Wang, G., et al., 2022. Microglia in depression: an overview of microglia in the pathogenesis and treatment of depression. J. Neuroinflammation 19, 132. https://doi.org/10.1186/s12974-022-02492-0.
Wang, M., Cao, J., Amakye, W.K., Gong, C., Li, Q., Ren, J., 2020. Mid infrared light treatment attenuates cognitive decline and alters the gut microbiota community in APP/PS1 mouse model. Biochem. Biophys. Res. Commun. 523, 60–65. https://doi.org/10.1016/j.bbrc.2019.12.015.
Wang, X., Li, X., Zuo, X., Liang, Z., Ding, T., Li, K., et al., 2021. Photobiomodulation inhibits the activa- tion of neurotoxic microglia and astrocytes by inhibiting Lcn2/JAK2-STAT3 crosstalk after spinal cord injury in male rats. J. Neuroinflammation 18, 256. https://doi.org/10.1186/s12974-021-02312-x.
Willner, P., 2017. The chronic mild stress (CMS) model of depression: history, evaluation and usage. Neurobiol Stress 6, 78–93. https://doi.org/10.1016/j.ynstr.2016.08.002.
Winter, G., Hart, R.A., Charlesworth, R.P.G., Sharpley, C.F., 2018. Gut microbiome and depression: what we know and what we need to know. Rev. Neurosci. 29, 629–643. https://doi.org/10.1515/revneuro-2017-0072.
Wong, M.-L., Inserra, A., Lewis, M.D., Mastronardi, C.A., Leong, L., Choo, J., et al., 2016. Inflammasome signaling affects anxiety- and depressive-like behavior and gut microbiome composition. Mol. Psychiatry 21, 797–805. https://doi.org/10.1038/mp.2016.46.
Yang, M., Yang, Z., Wang, P., Sun, Z., 2021. Current application and future directions of photobiomodulation in central nervous diseases. Neural Regen. Res. 16, 1177. https://doi.org/10.4103/1673-5374.300486.
Yien, Y.Y., Robledo, R.F., Schultz, I.J., Takahashi-Makise, N., Gwynn, B., Bauer, D.E., et al., 2014. TMEM14C is required for erythroid mitochondrial heme metabolism. J. Clin. Invest. 124, 4294–4304. https://doi.org/10.1172/JCI76979.
Yu, Z., Zhu, J., Wang, H., Li, H., Jin, X., 2021. Function of BCLAF1 in human disease (review). Oncol. Lett. 23, 58. https://doi.org/10.3892/ol.2021.13176.
Zhang, D., Shen, Q., Wu, X., Xing, D., 2021b. Photobiomodulation therapy ameliorates glutamatergic dysfunction in mice with chronic unpredictable mild stress-induced depression. Oxidative Med. Cell. Longev. 2021, 1–20. https://doi.org/10.1155/2021/6678276.
Zhang, W., Qu, W., Wang, H., Yan, H., 2021a. Antidepressants fluoxetine and amitriptyline induce alterations in intestinal microbiota and gut microbiome function in rats exposed to chronic unpredictable mild stress. Transl. Psychiatry 11, 131. https://doi.org/10.1038/s41398-021-01254-5.
Zhang, X., Wu, W., Luo, Y., Wang, Z., 2022. Transcranial Photobiomodulation therapy ameliorates perioperative neurocognitive disorder through modulation of mitochondrial function in aged mice. Neuroscience 490, 236–249. https://doi.org/10.1016/j.neuroscience.2021.12.033.
Zhang, Z., Shen, Q., Wu, X., Zhang, D., Xing, D., 2020. Activation of PKA/SIRT1 signaling pathway by photobiomodulation therapy reduces Aβ levels in Alzheimer's disease models. Aging Cell 19, e13054. https://doi.org/10.1111/acel.13054.
Zhu, Z., Wang, X., Song, Z., Zuo, X., Ma, Y., Zhang, Z., et al., 2022. Photobiomodulation promotes repair following spinal cord injury by restoring neuronal mitochondrial bioenergetics via AMPK/PGC-1α/TFAM pathway. Front. Pharmacol. 13, 991421 https://doi.org/10.3389/fphar.2022.991421.

Update

Journal of Affective Disorders

Volume 361, Issue , 15 September 2024, Page 799

DOI: https://doi.org/10.1016/j.jad.2024.07.001

Journal of Affective Disorders 361 (2024) 799–799

Contents lists available at ScienceDirect

Journal of Affective Disorders

journal homepage: www.elsevier.com/locate/jad

Corrigendum

Corrigendum to "Brain-gut photobiomodulation restores cognitive alterations in chronically stressed mice through the regulation of Sirt1 and neuroinflammation" [J. Affect. Disord. 354 (2024) 574–588 10.1016/j.jad.2024.03.075 (Jun 1, Epub 2024 Mar 14, PMID: 38490587)]

Anna Sancho-Balsells [a,b,c,**], Sara Borràs-Pernas [a,b,c], Francesca Flotta [a,b,c], Wanqi Chen [a,b,c], Daniel Del Toro [a,b,c], Manuel J. Rodríguez [a,b,c], Jordi Alberch [a,b,c,d], Aroa Relano-Gines [e], Guillaume Blivet [e], Jacques Touchon [f], Xavier Xifró [g,**], Albert Giralt [a,b,c,d,*]

[a] Departament de Biomedicina, Facultat de Medicina, Institut de Neurociències, Universitat de Barcelona, 08036 Barcelona, Spain
[b] Institut d'Investigacions Biomèdiques August Pi i Sunyer (IDIBAPS), 08036 Barcelona, Spain
[c] Centro de Investigación Biomédica en Red sobre Enfermedades Neurodegenerativas (CIBERNED), 28031 Madrid, Spain
[d] Production and Validation Centre of Advanced Therapies (Creatio), Faculty of Medicine and Health Science, University of Barcelona, 08036 Barcelona, Spain
[e] REGEnLIFE, 75008 Paris, France
[f] University of Montpellier, 34000 Montpellier, France
[g] New Therapeutic Targets Group, Department of Medical Science, Faculty of Medicine, Universitat de Girona, Girona, Spain

The authors regret to inform that they did not properly list Aroa Relano-Gines from RegenLife as one of the authors of the article. The authors also declare that Aroa Relano-Gines worked at RegenLife until September 16, 2022, and that she was involved with the work in terms of its visualization and conceptualization.

The authors would like to apologise for any inconvenience caused.

DOI of original article: https://doi.org/10.1016/j.jad.2024.03.075.
* Corresponding author at: Departament de Biomedicina, Facultat de Medicina, Institut de Neurociències, Universitat de Barcelona, Barcelona 08036, Spain.
** Corresponding authors.
E-mail addresses: annasanchobalsells@ub.edu (A. Sancho-Balsells), xavier.xifro@udg.edu (X. Xifró), albertgiralt@ub.edu (A. Giralt).

https://doi.org/10.1016/j.jad.2024.07.001

Available online 4 July 2024